Performace Evaluation of Maximum A-Posteriori Estimator in the Nakagami-m Fading MIMO Channels for m<1

Hamid Nooralizadeh[1], Mahyar Shirvanimoghaddam[2]
1- Department of Electrical Engineering, Islamshahr Branch, Islamic Azad University, Islamshahr, Iran.
Email: Hamid.Nooralizadeh@iau.ac.ir (Corresponding author)
2- School of Electrical and Computer Engineering, The University of Sydney, Australia.
Email: mahyar.shirvanimoghaddam@sydney.edu.au

ABSTRACT:
The Nakagami-m model has garnered significant attention in the literature as a versatile channel model suitable for describing channels experiencing varying degrees of fading, from severe to moderate. This model aligns closely with the characteristics observed in the majority of measured fading radio channels. The estimation of Nakagami-m fading in a multiple-input multiple-output (MIMO) channel poses a crucial challenge. Deriving the probability density function (pdf) for a Nakagami distribution random vector with correlated entries and developing closed-form classical and/or Bayesian estimators for a linear MIMO channel proves to be impractical. In this study, we simplify the analysis by assuming that the entries of the Nakagami fading random vector are uncorrelated. Consequently, the joint distribution of the channel vector entries is computed by multiplying the pdfs of the individual entries. Subsequently, the maximum a-posteriori (MAP) estimation of the channel entries is determined. Under the assumption of orthogonal training symbols, the obtained results lead to second-order nonlinear complex equations. To evaluate the performance of the MAP channel estimator in MIMO Nakagami-m frequency-flat fading channels, these nonlinear complex equations are solved numerically. The findings indicate that one-sided Gaussian fading represents the worst-case scenario, yet the channel estimation results surpass those of the least squares (LS) estimation. Additionally, fewer errors are observed in Rayleigh fading channel estimation. Furthermore, it is demonstrated that the performance of the MAP estimator improves with an increase in the Nakagami shape parameter. The numerical results affirm that the proposed estimator serves as a suitable method for estimating Nakagami-m fading in uncorrelated MIMO channels with m<1.

KEYWORDS: Nakagami-m Fading, One-sided Gaussian Fading, Rayleigh Fading, Maximum A-Posteriori Estimator.

1. INTRODUCTION

The focus on multiple input multiple output (MIMO) systems in wireless communications stems from their notable attributes of high capacity and diversity gain. Extensive research has demonstrated that in scenarios where the fades between pairs of transmit and receive antenna elements are independent and identically distributed (i.i.d.), the capacity of a Rayleigh distributed flat fading channel exhibits almost linear growth with the minimum number of transmitter and receiver antennas [1]-[3]. The study in [3] additionally highlights that Rician fading can enhance the capacity of a multiple antenna system, particularly when the transmitter possesses knowledge of the Rice factor. Furthermore, findings in [4], [5] reveal that in Nakagami-m fading, the MIMO channel capacity experiences an increase as the fading parameters are elevated.

To harness the benefits of MIMO systems, it is imperative that the receiver and/or transmitter possess access to channel state information (CSI). One prevalent method for determining MIMO CSI is through training-based channel estimation (TBCE) [6], [7]. The selection of optimal training signals typically involves exploring the minimization of

Paper type: Research paper
Received: 16 September 2023; revised: 25 November 2023; accepted: 7 December 2023; published: 1 March 2024
How to cite this paper: H. Nooralizadeh, M. Shirvanimoghaddam, **"Performace Evaluation of Maximum A-Posteriori Estimator in the Nakagami-m Fading MIMO Channels for m<1"**, *Majlesi Journal of Telecommunication Devices*, Vol. 13, No. 1, pp. 1-8, 2024.

the mean square error (MSE) of the linear MIMO channel estimator. Existing literature suggests that the optimal design of training sequences for MIMO channel estimation is intricately linked to the statistical characteristics of the channel, such as the fading model and the channel noise model.

While the Rayleigh model is commonly assumed for fading in many wireless communication systems, it is often conjectured that the MIMO channel fading follows a Rayleigh distribution. However, the Nakagami-m model proves to be a more suitable fit for the fading channel distribution. The Nakagami-m distribution fading model [8] stands out as one of the most versatile, demonstrating greater flexibility and accuracy in aligning with experimental data compared to Rayleigh, log-normal, or Rician distributions. This model is characterized by two parameters: the scale parameter and the shape parameter, denoted as 'm'. It incorporates the Rayleigh distribution when 'm' equals 1 and the one-sided Gaussian distribution when 'm' equals 1/2. Considered a versatile statistical distribution, Nakagami-m accurately models a variety of fading environments.

Various studies, including [4], [5], and [9], have delved into the modeling of Nakagami fading in MIMO channels. The challenge lies in determining the parameter 'm' during the estimation of the Nakagami probability density function (pdf). To effectively utilize the Nakagami-m distribution for modeling a given set of empirical data, it becomes necessary to ascertain or estimate the shape parameter from the data. The receiver, for optimal signal reception in Nakagami fading, also requires knowledge of this shape parameter. Different methods can be employed to estimate the required knowledge of channel statistics.

For example, in [10], the problem of estimating the Nakagami 'm' parameter is addressed using maximum likelihood (ML) estimation. In [11], a maximum a-posteriori (MAP) estimator is introduced for Nakagami-m fading parameter estimation. The derivation of the covariance matrix for correlated Nakagami-m fading channels is presented in [12]. Additionally, [13] introduces a copula-based method for estimating the Nakagami fading parameter in the received signal, which is subject to fading and contaminated by dependent noise.

In [7], [14], the authors proposed shifted scaled least squares (SSLS) and minimum mean square error (MMSE) estimators for the estimation of Rician fading in MIMO channels. Subsequently, in [15], the correlation between the channel Rice factor and the Nakagami shape parameter is utilized to formulate the MIMO channel covariance matrix. As a result, the SSLS and MMSE estimators can leverage the knowledge of Nakagami channel statistics, leading to an improvement in their performance. Numerical findings affirm the suitability of both estimators for Nakagami MIMO channel estimation, with the MMSE channel estimator demonstrating superior performance compared to the SSLS and least squares (LS) estimators. However, it is noted that the SSLS and MMSE estimators in [15] are specifically effective for scenarios where 'm' is greater than 1.

In this study, the MAP estimator is employed to estimate the Nakagami fading MIMO channel when 'm' is less than 1. The joint pdf of the channel vector entries is derived by multiplying the pdfs of the entries, assuming the vector entries are uncorrelated. Although the MAP estimation result does not yield a closed-form estimator, it leads to a set of nonlinear second-order complex equations. An algorithm is utilized to solve these equations and estimate the channel. Numerical results indicate an enhancement in the performance of the MAP estimator with an increase in the Nakagami shape parameter. Even in the most challenging scenario, where 'm' equals 0.5, the results are superior to those of the LS estimator.

The remainder of this paper is structured as follows: The next section introduces the system model of interest and outlines some assumptions regarding the fading process. Section 3 delves into the study of the MAP estimator. Numerical examples are presented in Section 4, while Section 5 serves as the conclusion for this paper.

2. THE SYSYEM MODEL

We consider a MIMO system with n_t transmitter and n_r receiver antennas. The frequency-flat block fading model is assumed for the MIMO channel. It means that the channel response is fixed within one block and can vary from one block to another one randomly. Each transmitted block contains training and data symbols. The frame structure is the same for all Tx antennas. Training and data symbols are located at the beginning and the end of the blocks, respectively. In practice, the channel is estimated using training symbols in the training phase, which will be used for data detection. To estimate the MIMO channel in each block, it is required that $n_p \geq n_t$ training signals are transmitted by each transmitter antenna. The $n_r \times n_p$ complex received signal matrix can be expressed as

$$\mathbf{Y} = \mathbf{HX} + \mathbf{V}, \quad (1)$$

where $\mathbf{X}$ and $\mathbf{V}$ are the complex n_t -vector of transmitted sequences on the n_t transmit antennas and n_r -vector of additive noise, respectively, and $\mathbf{H}$ is the $n_r \times n_t$ channel matrix. The elements of noise matrix are i.i.d. complex Gaussian random variables with zero mean and the variance σ_n^2 (i.e., $\mathcal{CN}(0, \sigma_n^2)$). The MIMO channel model (1) can be expressed in the following vector form:

$$\mathbf{y} = \widetilde{\mathbf{X}}\mathbf{h} + \mathbf{v} \quad (2)$$

where $\mathbf{y} = \text{vec}(\mathbf{Y})$, $\mathbf{v} = \text{vec}(\mathbf{V})$, $\widetilde{\mathbf{X}} = \mathbf{X}^T \otimes \mathbf{I}_{n_r}$, and $\mathbf{h} = \text{vec}(\mathbf{H})$. The notation $(\cdot)^T$ is reserved for the matrix transpose, $\otimes$ for the Kronecker product. $\mathbf{I}_r$ denotes the $r \times r$ identity matrix. The operand $\text{vec}(\cdot)$ stacks all the columns of the matrix argument into one tall column vector.

The entries of the channel matrix **H** in (1) or the vector **h** in (2) are assumed to be complex random variables with the following general form

$$h_{ij} = Re^{j\Theta} \quad (3)$$

where R is the envelope and Θ is the phase. The Nakagami-m fading envelope R has the following pdf [8]

$$f_R(r) = \frac{2\left(\frac{m}{\Omega}\right)^m r^{2m-1}}{\Gamma(m)} \exp\left(-\frac{m}{\Omega} r^2\right); \quad r \geq 0\,,\ m \geq 0.5 \quad (4)$$

Where $\Omega = E[R^2]$ is the expected value of the average power, and $m = \Omega^2/V[R^2]$ is the shaping parameter which controls the shape of the distribution, and $E[R^2]$ and $V[R^2]$ respectively denote the expectation and variance of R^2.

In (4), $\Gamma(\cdot)$ is the gamma function as follows

$$\Gamma(m) = \int_0^{+\infty} x^{m-1}\, e^{-x}\, dx \quad (5)$$

The mean and variance of R can be written as follows:

$$E[R] = \frac{\Gamma(m+1/2)}{\Gamma(m+1)} \sqrt{\frac{\Omega}{m}} \quad (6)$$

$$V[R] = \Omega\left(1 - \frac{1}{m}\left(\frac{\Gamma(m+1/2)}{\Gamma(m+1)}\right)^2\right) \quad (7)$$

The k-th moment of the Nakagami-m distribution is given by [10]

$$E[R^k] = \frac{\Gamma(m+k/2)}{\Gamma(m)} \left(\frac{\Omega}{m}\right)^{k/2} \quad (8)$$

In (3), the phase Θ is assumed to be uniformly distributed as follows:

$$f_\Theta(\Theta) = \frac{1}{2\pi}\,, \qquad -\pi \leq \Theta \leq \pi \quad (9)$$

The Nakagami-m distribution covers a wide range of fading conditions. For example, when m=0.5, it is reduced to a one-sided Gaussian distribution and when m=1, it is reduced to a Rayleigh distribution. In the limit when m→ ∞, the channel becomes static, and its corresponding pdf becomes an impulsive function located at $\sqrt{\Omega}$. For m < 1, the fading is more severe than the Rayleigh fading, and for values of m > 1, the fading is less severe. For the values of m > 1, the Nakagami-m distribution closely approximates the Rician distribution [15]. In the rest of the paper, we assume that m<1, unless otherwise specified.

3. MAP CHANNEL ESTIMATION

We assume that channels between each pair of transmit and receive antennas, i.e., h_{ij}'s, are independent. Therefore, the joint pdf of the entries of **h** is computed by multiplying the pdfs of the entries using (4) and (9) as

$$\boldsymbol{p}(\mathbf{h}) = \mathrm{C}\ \prod_{i=1}^{n_r}\prod_{j=1}^{n_t} |h_{ij}|^{2(m-1)}\ \exp\left(-\frac{m}{\Omega}\sum_{i=1}^{n_r}\sum_{j=1}^{n_t}|h_{ij}|^2\right) \quad (10)$$

Where $\mathrm{C} = \left(m^m/\pi\, \Omega^m\, \Gamma(m)\right)^{n_r\, n_t}$ and $h_{ij}, i = 1, 2, \ldots, n_r; j = 1, 2, \ldots, n_t$ are the elements of the channel matrix **H** in (1). The conditional pdf can be computed as

$$\boldsymbol{p}(\mathbf{y}|\mathbf{h}) = \frac{1}{\pi^{n_r\, n_t}\, \det(\mathbf{C_v})}\ exp\left(-\frac{1}{\sigma_n^2}\sum_{i=1}^{n_r}\sum_{j=1}^{n_t}|y_{ij} - z_{ij}|^2\right) \quad (11)$$

Where σ_n^2 is the variance of the elements of additive receiver noise matrix **V** in (1), $\mathbf{C_V}$ is the covariance matrix of the elements of the vector **v** in (2), $y_{ij}, i = 1, 2, \dots, n_r;\ j = 1, 2, \dots, n_t$ are the elements of the received signal matrix **Y** in (1), $z_{ij} = \sum_{n=1}^{n_t} h_{in}\, x_{nj}\,,\ i = 1, 2, \dots, n_r;\ \ j = 1, 2, \dots, n_t$, and $x_{ij}, i, j = 1, 2, \dots, n_t$ are the elements of the training matrix **X** in (1).

In MAP, the channel is estimated in order to maximize $\boldsymbol{p}(\mathbf{h})\ \boldsymbol{p}(\mathbf{y}|\mathbf{h})$ as follows:

$$\hat{\mathbf{h}}_{MAP} = \underset{\mathbf{h}}{\operatorname{argmax}}\ \left(\boldsymbol{p}(\mathbf{h})\ \boldsymbol{p}(\mathbf{y}|\mathbf{h})\right), \qquad (12)$$

or equivalently,

$$\hat{\mathbf{h}}_{MAP} = \underset{\mathbf{h}}{\operatorname{argmax}}\ (\ln \boldsymbol{p}(\mathbf{h}) + \ln \boldsymbol{p}(\mathbf{y}|\mathbf{h})). \qquad (13)$$

Using (10), (11) and by differentiating $\ln \boldsymbol{p}(\mathbf{h}) + \ln \boldsymbol{p}(\mathbf{y}|\mathbf{h})$ with respect to $h_{kl},\ k = 1, 2, \dots, n_r;\ \ l = 1, 2, \dots, n_t$ and setting the results equal to zero, $n_r n_t$ complex second-order equations are obtained as

$$-(m-1) + \frac{m}{\Omega}\,|h_{kl}|^2 - \left(\sum_{j=1}^{n_t} x_{lj}\overline{y}_{kj}\right) h_{kl}$$
$$-\sum_{j=1}^{n_t}\sum_{\substack{n=1\\ n\neq l}}^{n_t} x_{lj}\overline{x}_{nj}\,\overline{h}_{kn}h_{kl} + \left(\sum_{j=1}^{n_t}\left|x_{lj}\right|^2\right)|h_{kl}|^2 = 0$$

$$k = 1, 2, \dots, n_r;\ \ l = 1, 2, \dots, n_t \qquad (14)$$

Where $\overline{(.)}$ denotes the complex conjugate. Assuming that a training matrix **X** with orthogonal rows is used here, we have

$$\sum_{j=1}^{n_t} x_{lj}\overline{x}_{nj} = 0 \qquad for\ l, n = 1,2, \dots, n_t \qquad (15)$$

Using (15), it is straightforward to show that under orthogonal training for the MAP estimator, (14) reduces to

$$a_l|h_{kl}|^2 - b_{kl}\,h_{kl} - (m-1) = 0$$

$$k = 1, 2, \dots, n_r;\quad l = 1, 2, \dots, n_t \qquad (16)$$

Where,

$$a_l = \frac{m}{\Omega} + \sum_{j=1}^{n_t}\left|x_{lj}\right|^2, \qquad (17)$$

$$b_{kl} = \sum_{j=1}^{n_t} x_{lj}\overline{y}_{kj} \qquad (18)$$

Generally, the second-order equations of (16) have two roots for any *k*, *l*. The roots that maximize the function $\boldsymbol{p}(\mathbf{h})\ \boldsymbol{p}(\mathbf{y}|\mathbf{h})$ are chosen. Suppose $h_{kl} = h_{kl_R} + jh_{kl_I}$, where h_{kl_R} is the real part of h_{kl} and h_{kl_I} is the imaginary part of h_{kl}. Also, suppose $b_{kl} = b_{kl_R} + jb_{kl_I}$, where b_{kl_R} is the real part of b_{kl} and b_{kl_I} is the imaginary part of b_{kl}. Substituting them in (16) and with some calculations, for $k = 1, 2, \dots, n_r;\ \ l = 1, 2, \dots, n_t$ we will have

$$d_{kl}\left(h_{kl_R}\right)^2 + e_{kl}\,h_{kl_R} - (m-1) = 0, \qquad (19)$$

$$h_{kl_I} = -h_{kl_R}\,\frac{b_{kl_I}}{b_{kl_R}}\ . \qquad (20)$$

Where,

$$d_{kl} = a_l\left(1 + \left(\frac{b_{kl_I}}{b_{kl_R}}\right)^2\right), e_{kl} = -\left(b_{kl_R} + \frac{\left(b_{kl_I}\right)^2}{b_{kl_R}}\right). \qquad (21)$$

In order to estimate the channel matrix **H**, We use Algorithm 1, as follows:

Algorithm 1: The MAP estimation's steps.

Step 1: Solve the second order equation (19) for $k = 1$ and $l = 1, 2, \dots, n_t$ (there are two roots for any k, l, generally)
Step 2: Calculate (20) for $k = 1, l = 1, 2, \dots, n_t$ and for both roots of (19)
Step 3: Calculate $h_{kl} = h_{kl_R} + jh_{kl_I}$ for $k = 1$ and $l = 1, 2, \dots, n_t$ and for both roots of (19)
Step 4: Calculate the function
$f(k) = \sum_{j=1}^{n_t} ln|h_{kj}|^{2(m-1)} - \frac{m}{\Omega}\sum_{j=1}^{n_t}|h_{kj}|^2 - \sum_{j=1}^{n_t}|y_{kj} - z_{kj}|^2$
for 2^{n_t} combinations of roots obtained in step 3 and choose a combination of roots that maximizes $f(k)$
Step 5: Repeat steps 1-4 for $k = 2, \dots, n_t$

In Step 4 of the Algorithm 1, we are using the following relation

$$\ln \boldsymbol{p}(\mathbf{h}) + \ln \boldsymbol{p}(\mathbf{y}|\mathbf{h}) = \ln \mathrm{C} + \ln \mathrm{B} + \sum_{k=1}^{n_t} f(k) \qquad (22)$$

Where $\mathrm{B} = 1/\pi^{n_r n_t} \det(\mathbf{C_v})$, and B, C are independent of h_{kl}.

4. SIMULATION RESULTS

In this section, the performance of the MAP estimator is numerically evaluated. To measure the accuracy of the channel estimation, we use the normalized mean square error (NMSE) defined as follows

$$NMSE = \frac{E\{\|\mathbf{h} - \hat{\mathbf{h}}\|_F^2\}}{E\{\|\mathbf{h}\|_F^2\}} \qquad (23)$$

For simulations, we generate samples of MIMO channels using the Nakagami-m distribution. For the training sequences, we use the orthogonal sequences proposed in [6] ad [7]. For each signal-to-noise ratio (SNR), we run 5000 simulations and average find the NMSE using (23).

Fig. 1 shows NMSE of the LS estimator [10] and the MAP channel estimator (algorithm 1) with orthogonal training versus signal to noise ratio (SNR) for various Nakagami shape parameters when n_r= n_t=1. As it is expected, the LS estimator can not exploit the knowledge of m, a phenomenon that is confirmed in [15]. In [6], [7] and [15] it was shown that the LS estimator does not require any knowledge of the channel and that the performance of the LS estimator is independent of the channel shape parameter, m, and the correlation coefficients. Here, we use the LS estimator as a benchmark for comparison. It is observed that one-sided Gaussian distribution (m = 0.5) is the worst case for the MAP estimation, however, the result is still better than LS estimation. Moreover, by increasing m the performance of the MAP estimator improves, especially at low SNRs.

Figs. 2 and 3 show the NMSE of the LS and MAP estimators for higher number of transmitter and receiver antennas. As can be seen, at high SNRs, the performances of the MAP estimator for different values of m are similar particularly for lower number of transmitter and receiver antennas. It is notable that in the special case of m = 1, i.e Rayleigh fading, the MAP estimator is the same as the MMSE estimator of [6] for low correlations.

Figs. 4, 5, and 6 compare the NMSE of the MAP channel estimator versus SNR for various number of transmitter and receiver antennas when m=0.5, m = 0.75, and m=1, respectively. As expected, increasing the number of transmitter and receiver antennas results in higher channel estimation error.

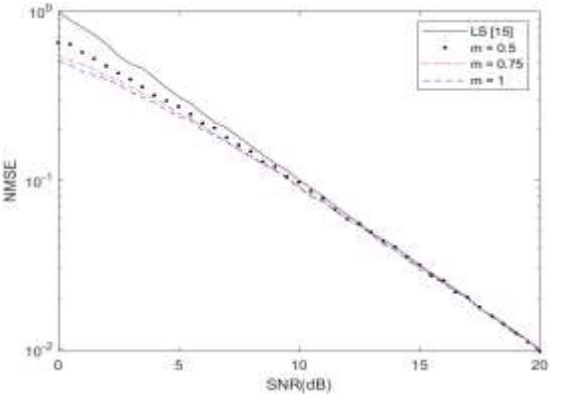

Fig. 1. NMSE of the LS and MAP estimators vs. SNR for various Nakagami shape parameters and $n_r = n_t = 1$.

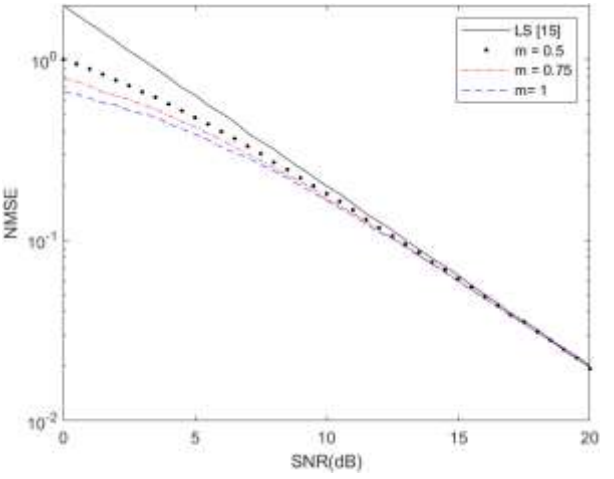

Fig. 2. NMSE of the LS and MAP estimators vs. SNR for various Nakagami shape parameters and $n_r = n_t = 2$.

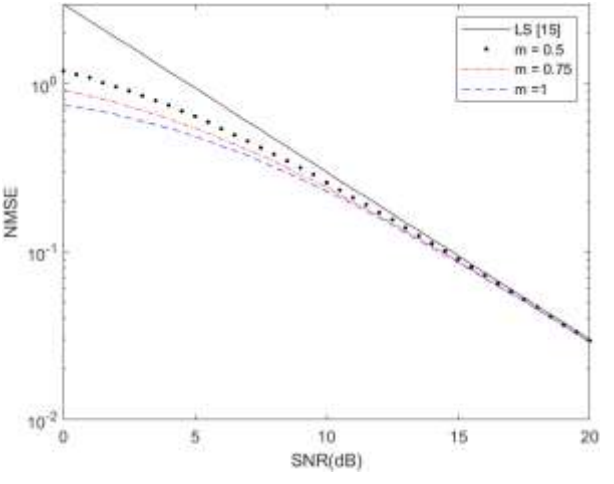

Fig. 3. NMSE of the LS and MAP estimators vs. SNR for various Nakagami shape parameters and $n_r = n_t = 3$.

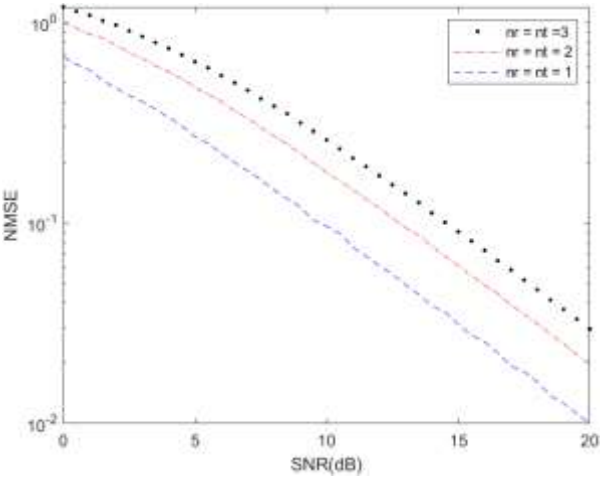

Fig. 4. NMSE of the MAP estimator vs. SNR for various number of antennas $n_r = n_t$ and m = 0.5.

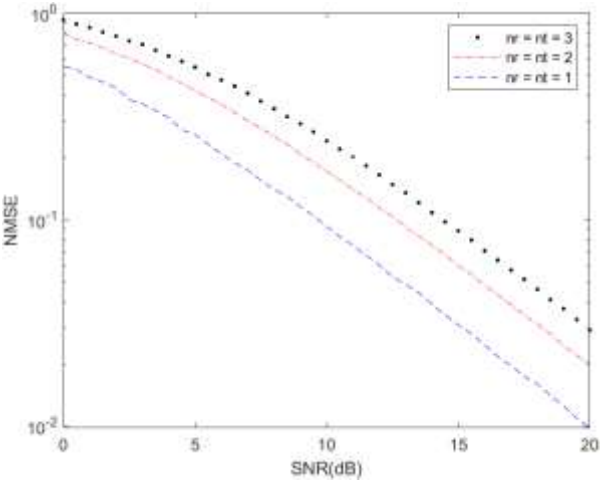

Fig. 5. NMSE of the MAP estimator vs. SNR for various number of antennas $n_r = n_t$ and m = 0.75.

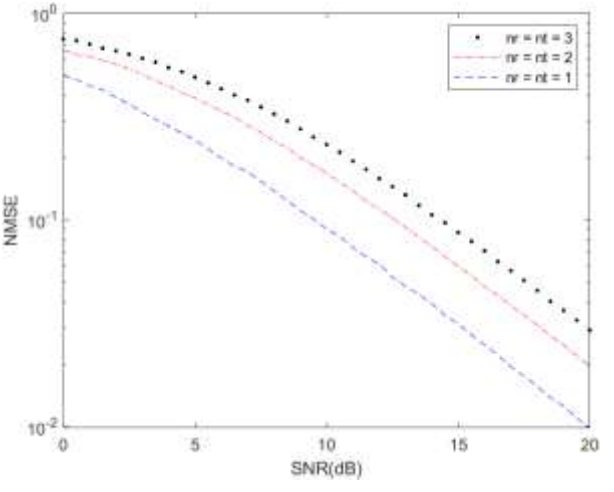

Fig. 6. NMSE of the MAP estimator vs. SNR for various number of antennas $n_r = n_t$ and m = 1.

5. CONCLUSIONS

This paper introduces the MAP estimator for estimating Nakagami fading in uncorrelated MIMO channels with m < 1. The proposed approach yields a set of second-order nonlinear equations characterized by complex coefficients. An algorithm is employed to solve these equations and obtain the channel coefficients. As anticipated, an increase in the Nakagami shape parameter contributes to an enhancement in channel estimation accuracy. Remarkably, the MAP estimation results outperform classical LS estimation, even under severe fading conditions, such as when m=0.5. In the special case where m=1, corresponding to the Rayleigh fading model, the MAP approach presented in this paper aligns with the MMSE technique from [6] for uncorrelated channel scenarios. It is noteworthy that for m > 1, the channel follows a Rician distribution and experiences less severe fading. Previous work in [15] has addressed the estimation of this channel type, and the results align with the findings presented in this article. Nakagami fading is recognized as a suitable model for wireless environments, with the Nakagami-m distribution often providing the best fit for land-mobile and indoor-mobile multipath propagation.

REFERENCES

[1] D. Tse and P. Viswanath, Fundamentals of wireless communication, Cambridge University Press, 2005.
[2] I.E. Telatar, **"Capacity of multi-antenna Gaussian channels,"** *European Trans. Telecommunications*, vol. 10, no. 6, pp. 585–595, Nov. 1999.
[3] S.K. Jayaweera and H.V. Poor, **"On the capacity of multiple-antenna systems in Rician fading,"** *IEEE Trans. Wireless Communications*, vol. 4, issue 3, pp. 1102-1111, May 2005.
[4] M. H. Gholizadeh, H. Amindavar, and J. A Ritcey, **"On the capacity of MIMO correlated Nakagami-m fading channels**

using copula," *EURASIP Journal on Wireless Communications and Networking*, 2015(1).

[5] T. M. Hoang, B. C. Nguyen, X. N. Tran and L. T. Dung, "**Outage probability and ergodic capacity of user clustering and beamforming MIMO-NOMA relay system with imperfect CSI over Nakagami-m fading channels**," *IEEE Systems Journal*, vol. 15, no. 2, pp. 2398-2409, June 2021.

[6] M. Biguesh and A.B. Gershman, **"Training-based MIMO channel estimation: A study of estimator tradeoffs and optimal training signals,"** *IEEE Trans. Signal Processing*, vol. 54, no.3, pp. 884-893, March 2006.

[7] H. Nooralizadeh and S. Shirvani Moghaddam, **"A novel shifted type of SLS estimator for estimation of Rician flat fading MIMO channels,"** *Signal Process*, vol. 90, issue 6, pp. 1887–1894, June 2010.

[8] M. Nakagami, The m-distribution - a general formula of intensity distribution of rapid fading, in Statistical Methods in Radio Wave Propagation, W. C. Hoffman, Ed. Oxford, England: Pergamon, 1960.

[9] R. Mesleh, O. Badarneh and A. Younis, "**Nakagami-m MIMO channel model**," 2022 9th International Conference on Electrical and Electronics Engineering (ICEEE), Alanya, Turkey, 2022, pp. 280-284.

[10] J. Cheng and N.C. Beaulieu, **"Maximum-Likelihood based estimation of the Nakagami m parameter,"** *IEEE Communications Letters*, vol. 5, no. 3, pp. 101-103, March 2001.

[11] P. L. Ramos, F. Louzada and E. Ramos, "**An efficient, closed-form MAP estimator for Nakagami-m fading parameter**," *IEEE Communications Letters*, vol. 20, no. 11, pp. 2328-2331, Nov. 2016.

[12] J.C. Lin, and H.V. Poor, **"A systematic approach to deriving the covariance matrix of correlated Nakagami-m fading channels,"** *IEEE Trans. Vehicular Technology*, vol. 69, issue 2, pp. 1612-1625, February 2020.

[13] M. H. Gholizadeh, H. Amindavar and J. A Ritcey, **"Analytic Nakagami fading parameter estimation in dependent noise channel using copula,"** *EURASIP Journal on Advances in Signal Processing*, December 2013.

[14] H. Nooralizadeh, **"Advantages of multiple-estimation in the frequency selective block fading MIMO environments,"** *Majlesi Journal of Electrical Engineering*, vol. 9, no. 3, pp. 17-30, September 2015.

[15] H. Nooralizadeh, **"The performance of SSLS and MMSE estimators on the Nakagami-m fading MIMO channels"** In proc. 12th Majlesi Conference on Electrical Engineering. August 2023.

Using The Gray Wolf Optimization Algorithm for Community Detection

Malihe Ghasemzade[1], Mohammad Amin Ghasemzadeh[2]
1- Department of Metallurgical Engineering, Karaj Branch, Islamic Azad University, Karaj, Iran.
2- Master of Electrical Engineering, CQUniversity, Melbourne, Australia.

ABSTRACT:
In today's world, networks play a very important role in people's lives. One of the important issues related to networks is the issue of detecting communities. These communities are also called groups and clusters. Communities include nodes that are closely related to each other. Most of the nodes that are members of a community have common properties. In social networks, it is important to detect the community in order to analyze the network and it is a very important tool to understand the information of the network and its structure. Studying community detection has garnered significant interest in last few years, leading to the development of numerous algorithms in this area. this research, we used the gray wolf meta-heuristic algorithm and improved it with operators such as mutation, combination, and local search, and also improved the final solution of the gray wolf algorithm with the label propagation algorithm to detect communities. Experiments showed that the proposed method has high accuracy and also due to the applied techniques, the problem converges to the best solution very quickly.

KEYWORDS: Community Detection, Gray Wolf Algorithm, Label Propagation Algorithm, Optimization.

INTRODUCTION

Networks play an important role in today's human societies, and since the data in many different fields can be naturally converted into graph structure, it can be claimed that this network is present in all fields. [1]. Many of the above systems and networks can be modeled as a network, where the links of the networks represent the relationships between the internal components of the system (nodes). In different domains, network links can represent different types of relationships such as human friendship, organizational structure, physical proximity of animals, infrastructure connections, web links [2]. Technological networks, including the Internet, electricity networks, telephone networks and road networks are an important part of daily life. Some of the popular networks include social media and online social networking sites like Facebook.

In general, one of the things that we see a lot in nature and has existed since the beginning of creation, is the existence of different communities (groups). A community, also known as a module or cluster, is a collection of nodes that are almost interconnected and have an inherently network-specific structure. Identifying Nodes that belong to the same community frequently exhibit similar characteristics, such as sharing common functions, interests, or goals. Therefore, the detection of communities is a significant consideration in network analysis [3]. Therefore, the study of various aspects of these networks has been taken into consideration by many researchers. An important topic in the analysis of social networks is the exploration of group identification. A significant aspect of social networks involves understanding their formation. This has led to the emergence of clusters at the graph level. A cluster is a collection of vertices with a higher number of internal edges than external edges linking these vertices to vertices in other clusters. [4].

So far, Numerous algorithms have been suggested for identifying communities, and these algorithms can be broadly categorized as either general or local methods. [5]. General methods have high complexity [6]. Hence, the local group detection methods have been developed as a solution for the unavailability of social networks and the complexity of calculations. Local algorithms are less accurate than general algorithms due to the use of local information. Also, getting stuck in local minima (maxima) is one of the most important problems faced by this group of algorithms, and for this reason, these algorithms often do not recover all the vertices of a group and stop after recovering a limited number of vertices. Therefore, having an efficient method to overcome these shortcomings is strongly felt.

Paper type: Research paper
Received: 5 October 2023; revised: 28 November 2023; accepted: 13 December 2023; published: 1 March 2024
How to cite this paper: M. Ghasemzade, M. A. Ghasemzadeh, **"Using The Gray Wolf Optimization Algorithm for Community Detection"**, *Majlesi Journal of Telecommunication Devices*, Vol. 13, No. 1, pp. 9-15, 2024.

In this research, our goal is to present a meta-heuristic algorithm method and improve it with mutation and combination operators and local search and integrate it with the label propagation algorithm with the aim of faster convergence and better performance to detect communities in social networks.

LITERATURE

Studying community detection has garnered significant interest in last few years, leading to the development of numerous algorithms in this area. The first algorithm presented in community detection was the GN algorithm proposed by Girvan and Newman, which was based on the idea of graph partitioning. In this algorithm, it uses the concept of connection centrality to find adjacent edges. Despite the improvements, the algorithm has a high time complexity. [7]

Clauset et al introduced a fast greedy algorithm that works with modularity. [8] At first, each node is assigned to a cluster. Then, the amount of modularity change ΔQ ij in the combination of clusters is calculated. The combinations that have the highest increase are merged and become a new cluster. Modularity change is calculated only for clusters that have been affected. Once again, the combination with the highest value is merged. This process continues until all nodes become several large communities. This process is both memory efficient and fast in terms of time. This is because the modularity change is only updated for the affected clusters. The time complexity of the algorithm is close to linear. Zhao et al presented the CL Anet method, which is used for modularity maximization along with a local limiter using learning automata. [9]. An article by Panizo et al. [10] titled "Genetic Algorithm with Local Search Based on the label Propagation for detecting dynamic communities" was published. The idea used in this article is to combine the label propagation algorithm with the genetic algorithm. In 2022, an article [11] titled "An algorithm based on gray wolf optimization and balanced modularity for community detection in social networks" was published by Ehsan Jokar et al. In this paper, to improve the gray wolf algorithm, they used the label propagation algorithm to generate the initial population and applied the local search operator to the best solution of the algorithm. Fatemeh Besharatnia et al. [12] used the gray wolf algorithm to detect communities in static networks. In their method, they used the modularity criterion as the objective function. The comparison of the results of their method with other famous algorithms showed that their method has good performance and accuracy.

Raghavan [13] was the first one who used the label propagation algorithm for the problem of community detection. The purpose of this algorithm is to divide the network without knowing the size and number of communities. The steps of the standard algorithm are as follows: First, all the nodes are given a unique initial label. Then a random visit list is generated for all nodes. The label of each node is updated according to the label of neighboring nodes. The tag that has the highest number of repetitions in the neighbors is tied to it, and if there are several tags with the same number of repetitions, the tag is randomly selected from among them. This operation of updating labels will continue until the label of each node is equal to the label of most of its neighbors. Finally, the nodes that have the same label are placed in a community. The time complexity of the label propagation algorithm is close to linear, and hence it is a suitable candidate for detecting communities in social networks.

RESEARCH METHODOLOGY

Our goal in this research is to introduce a new model for detecting communities using the meta-heuristic algorithm of the gray wolf optimizer in social networks and improve it with mutation and combination operators and local search and combine it with the label propagation algorithm that has linear time complexity [14] and is one of the famous and fast algorithms in the issue of community detection with the aim of detecting common nodes. In the following, the performance of this algorithm has been evaluated by applying it to the problem of community detection and evaluating the quality of communities.

GRAY WOLVES METAHEURISTIC ALGORITHM

Inspired by the social life and hunting of gray wolves, The gray wolf algorithm employs four categories of wolves to model hierarchical leadership patterns. Gray wolves demonstrate a highly structured social hierarchy, with the alpha pair consisting of one male and one female serving as leaders. The alpha is primarily tasked with making decisions related to hunting, resting locations, and wake-up times, and their directives are followed by the rest of the group. However, instances of democratic behavior have been noted, wherein the alpha defers to other pack members. During group assemblies, the alpha's status is affirmed as the rest of the pack holds its tail down in recognition. Because the group is required to comply with the alpha's commands, only alpha wolves have the privilege of selecting a mate within the pack. It is intriguing to note that the alpha is not always the most physically dominant group member, but rather excels in group management. This serves to demonstrate that the organization and discipline within a group hold greater significance than sheer power. [15, 18].

The gray wolf hierarchy's second tier is occupied by the beta, who serves as the advisor to the alpha and organizes the group's activities. The beta then ensures the implementation of the alpha's directives across the group and provides feedback to the alpha. Within the gray wolf structure, the omega holds the lowest rank and assumes the role of the victim, being the last among the wolves to partake in eating. Any wolf not classified as an alpha, beta, or omega is referred to as a subordinate (or delta in certain sources). The delta wolf is required to report to the alpha and beta, but holds dominance over the omega.

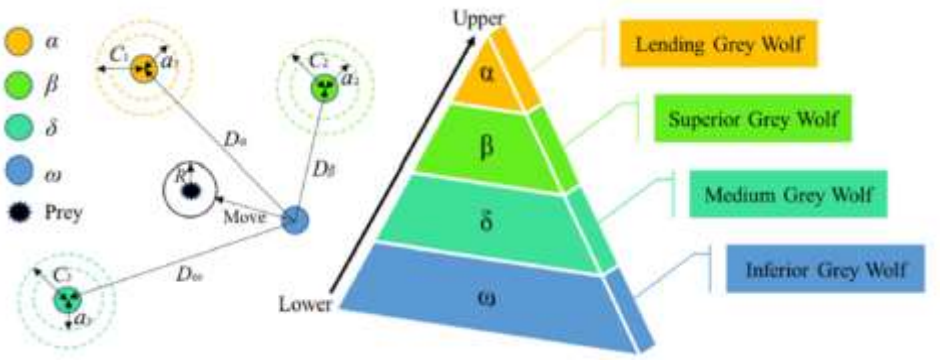

Fig. 1. Schematic diagram of GWO. [19].

In addition to the social hierarchy, gray wolf hunting has three stages: tracking, chasing and approaching the prey. To model the social hierarchy of wolves, we consider alpha as the best answer and beta and delta as the second and third among the best solutions. We consider the rest of the candidate solutions to be Omega. Optimization is driven by alpha, beta and delta and the fourth group follows these three groups. The modeling of wolves' siege behavior uses relations 1 and 2:

$$\vec{D} = |\vec{C} \cdot \vec{X_p}(t) - \vec{X}(t)| \quad (1)$$

$$\vec{X}(t+1) = \vec{X_p}(t) - \vec{A} \cdot \vec{D} \quad (2)$$

Where, t is the current iteration number, A and C are coefficient vectors, Xp is the position vector of the prey and X is the position vector of a wolf. To calculate vectors A and C, relations 3 and 4 are used.

$$\vec{A} = 2\vec{a} \cdot \vec{r_1} - \vec{a} \quad (3)$$

$$\vec{C} = 2 \cdot \vec{r_2} \quad (4)$$

The vector a decreases from 2 to 0 linearly during the iteration period in both exploration and exploitation phases. R is a random vector between 0 and 1. Due to the randomness of the vectors r_1 and r_2, wolves can change their position in the space containing the prey randomly and using relations 5 and 6. This idea can be expanded to apply to an n-dimensional search space, where the gray wolves navigate around the optimal solution found in a greater number of dimensions compared to the dimensions of a cube.

Alpha wolves typically lead gray wolf hunts, with occasional participation from beta and delta wolves. To emulate this behavior, we store the three best solutions acquired and compel other search agents to adjust their position based on the location of the top search agents according to equation 7.

In this algorithm, the implementation of the exploit or attack phase, which happens when the prey is stopped, is done by reducing the value of the variable a from 2 to 1. The value of A is also dependent on a, so it decreases.

$$\begin{aligned} \vec{D_\alpha} &= |\vec{C_1} \cdot \vec{X_\alpha} - \vec{X}| \\ \vec{D_\beta} &= |\vec{C_2} \cdot \vec{X_\beta} - \vec{X}| \\ \vec{D_\delta} &= |\vec{C_3} \cdot \vec{X_\delta} - \vec{X}| \end{aligned} \quad (5)$$

$$\begin{aligned} \vec{X_1} &= \vec{X_\alpha} - \vec{A_1} \cdot \vec{D_\alpha} \\ \vec{X_2} &= \vec{X_\beta} - \vec{A_2} \cdot \vec{D_\beta} \\ \vec{X_3} &= \vec{X_\delta} - \vec{A_3} \cdot \vec{D_\delta} \end{aligned} \quad (6)$$

$$\vec{X(t+1)} = \frac{\vec{X_1} + \vec{X_2} + \vec{X_3}}{3} \quad (7)$$

As the value of A decreases, wolves are forced to attack prey. An identification phase is also provided to avoid getting stuck in the local minimum trap. Wolves move away from each other to search for prey and come close to each other to attack and cooperate. To simulate this divergence, we use vector A with random values larger than 1 or smaller than -1 as shown in Fig. 2.

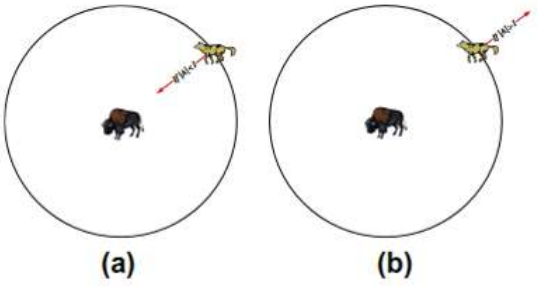

Fig 2. Attacking prey versus searching for prey.

Another influencing factor is the process of identifying the C value. The value of this random numerical vector is in the interval of [0, 2] and this random value intensifies (C>1) or weakens (C<1) the influence of the position of the prey in determining the distance. This vector can also be considered as the effect of obstacles that prevent approaching the prey in nature.

Initialize the grey wolf population X_i (i = 1, 2, ..., n)
Initialize a, A, and C
Calculate the fitness of each search agent
X_α=the best search agent
X_β=the second best search agent
X_δ=the third best search agent
while *(t < Max number of iterations)*
  for *each search agent*
    Update the position of the current search agent by equation (3.7)
  end for
  Update a, A, and C
  Calculate the fitness of all search agents
  Update X_α, X_β, and X_δ
  t=t+1
end while
return X_α

Fig. 3. Pseudo code of the GWO algorithm.

THE PROPOSED ALGORITHM

Detecting communities is very important and vital in extracting the network format. A large number of proposed algorithms are known to date, one of their most important problems is the scalability of these types of algorithms. In this research, gray wolf meta-heuristic algorithm has been used along with applying techniques such as: mutation, combination and local search operators and its combination with label propagation algorithm, so that our proposed method converges to the best possible solution with better speed and accuracy than other algorithms.

EVALUATION CRITERIA

The quality of communities obtained by the algorithm is obtained using the modularity criterion provided by Girvan-Newman.

$$Q(C) = \frac{1}{2m}\sum_{i,j}\left(A_{ij} - \frac{k_i k_j}{2m}\right)\delta(C_i, C_j)$$

Where A is the adjacency matrix of the network, ki represents the degree of node i, and m is the number of edges in the network. The function δ has a value of one for two vertices inside a community and zero otherwise. If the number

of outcluster edges is as many random graphs, then Q will be zero. Q values close to 1 indicate a strong community structure. In practice, this value is between 0.3 and 0.7 for the structure of strong communities. [16,20].

DATASET

The specifications of the dataset used in this research are as follows.

Table 1. Test network specifications

Oriented	The number of communities	The number of edges	The number of nodes	**Dataset**
No	۲	۱۵۹	۶۲	Dolphin Social Network

DOLPHIN BOTTLENOSE NETWORK

The Bottlenose Dolphins network consists of 62 nodes and 159 edges that reflect the social behavior between dolphins. The network was created by David Lusseau, a biologist who spent 7 years scrutinizing dolphin behavior and mining data for the network. In this way, if a connection is established between two dolphins, a connection is created. The figure below shows the basic template of the Dolphin Network community [17].

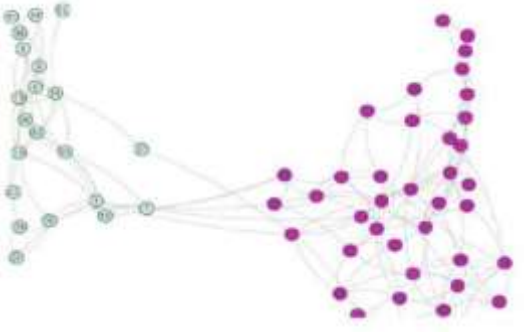

Fig. 4. Dolphin network graph.

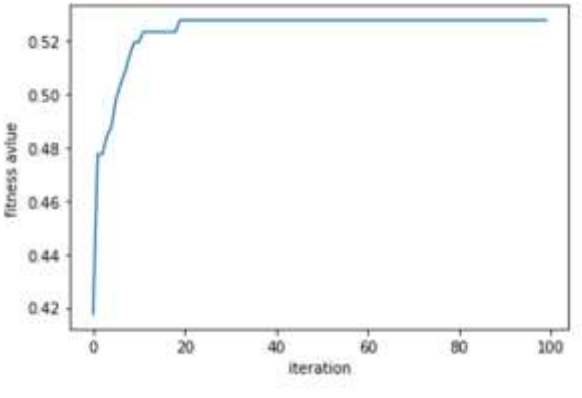

Fig. 6. Algorithm test result.

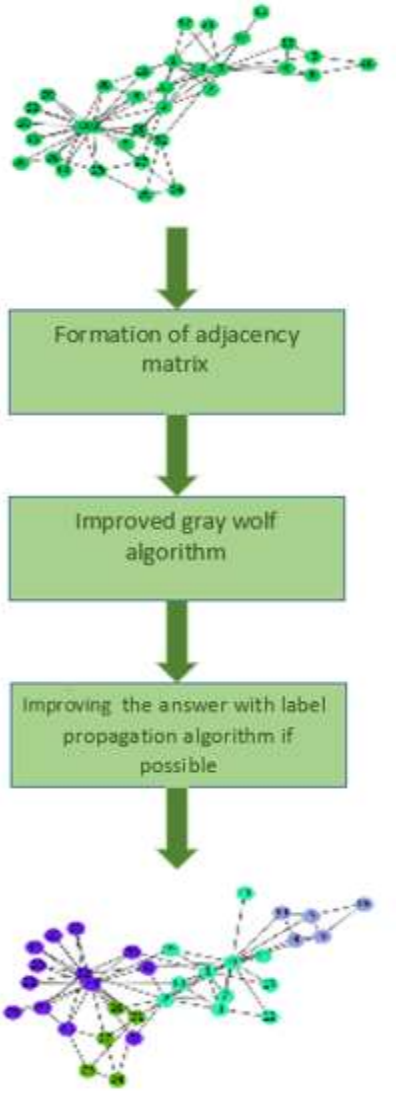

Fig. 5. Summary of the proposed method.

RESEARCH FINDINGS

In this article, by using the gray wolf meta-heuristic algorithm and applying several techniques on it to improve the algorithm, we were able to achieve better performance and modularity than other methods.

In the implementation of our proposed method (GWO-LP), we created the gray wolf algorithm along with the changes we considered to improve it in the form of a function called GWO. Before calling the GWO function, it is necessary to create the adjacency matrix of the desired graph in the form of a two-dimensional matrix. After creating the adjacency matrix of the desired data set, it is enough to call the GWO function to perform the community detection operation. After the gray wolf algorithm is fully implemented, we apply the label propagation algorithm to the labels obtained by the gray wolf algorithm, with the aim of increasing the modularity.

In this step, we traverse all the nodes of the graph by the label propagation algorithm. In the label propagation algorithm, we relabel nodes that overlap, that is, nodes that can belong to multiple communities, if possible, based on the importance of neighboring nodes. After changing the labels by the label propagation algorithm, if we reach a higher modularity, we accept the labels of the label propagation algorithm as the final solution.

The results obtained from running the algorithm on the Dolphin dataset are reported in the table below. Also, the images of the convergence diagram and the discovered communities are specified below.

Table 2. Results of running the algorithm on the dolphin dataset

Modularity	The number of gray wolves	The number of repetitions	**Dataset**
0.5277	80	100	dolphin

Table 3. Test results

GWO-LP	**BGLL**	**MODPSO**	**CNM**	**Ga-net**	**NLPSO-D**	**Newman**	
0.5277	0.526	0.5268	0.4950	0.4946	0.5144	0.465	**Dolphins**

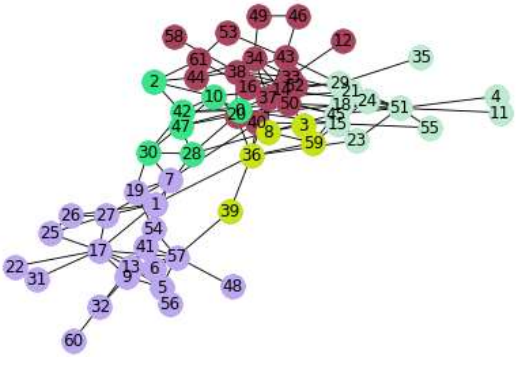

Fig. 7. The structure of communities detected in Dolphin graph.

CONCLUSION

So far, many algorithms have been presented for the topic of community detection, most of them have problems such as unstable results, lack of scalability, long execution time, etc. In this research, we proposed an improved gray wolf algorithm for community detection. We also used the label propagation algorithm, which is considered a fast algorithm, to improve the solution obtained by the gray wolf algorithm. By examining the results, we have come to the conclusion that the presented model achieves higher modularity than other meta-heuristic algorithms. Also, due to the use of existing edges, between graph nodes in the construction of the initial population and the use of various operators such as mutation, combination and local search, etc., the algorithm has faster convergence than other methods.

REFERENCES

[1] Newman, M.E., **"The structure and function of complex networks".** *SIAM review*, 2003. 45(2): p. 167-256.

[2] Ellison, N.B., **"Social network sites: Definition, history, and scholarship".** *Journal of Computer-Mediated Communication*, 2007. 13(1): p. 210-230.

[3] Xu, T., et al., **"Generative models for evolutionary clustering".** *ACM Transactions on Knowledge Discovery from Data (TKDD)*, 2012. 6(2): p. 7.

[4] Barber, M.J., **"Modularity and community detection in bipartite networks".** *Physical Review* E, 2007. 76(6): p. 066102.

[5] Plantié, M. and M. Crampes, **"Survey on social community detection",** *in Social media retrieval*. 2013, Springer. p. 65-85.

[6] Bagrow, J.P. and E.M. Bollt**, "Local method for detecting communities".** *Physical Review* E, 2005. 72(4): p. 046108.

[7] Girvan, M. and M.E. Newman, **"Community structure in social and biological networks".** *Proceedings of the national academy of sciences*, 2002. 99(12): p. 7821-7826.

[8] Clauset, A., M.E. Newman, and C. Moore, **"Finding community structure in very large networks"**. *Physical review E*, 2004. 70(6): p. 066111.

[9] Zhao, Y., Jiang, W., Li, S., Ma, Y., Su, G., & Lin, X. (2015**). "A cellular learning automata based algorithm for detecting community structure in complex networks"**. *Neurocomputing*, 151, 1216- 1226

[10] Panizo, A., G. Bello-Orgaz, and D. Camacho. **"A genetic algorithm with local search based on label propagation for detecting dynamic communities".** *in Intelligent Distributed Computing XII*. 2018. Springer.

[11] Jokar, E., M. Mosleh, and M. Kheyrandish, **"GWBM: an algorithm based on grey wolf optimization and balanced modularity for community discovery in social networks".** *The Journal of Supercomputing*, 2022. 78(5): p. 7354-737.۷

[12] F. Basharatnia, A .Talebpour, and S .Ali Akbari, **"Community detection in static social networks using gray wolf optimization algorithm ."***Bi-quarterly Journal of Soft Engineering and Computer Engineering*/Vol. 4, No. 1, Spring and Summer 1۲۰۱۷ .

[13] Raghavan, U.N., R. Albert, and S. Kumara, **"Near linear time algorithm to detect community structures in large-scale networks"**. *Physical review* E, 2007. 76(3): p. 036106.

[14] ZhuЃ, X. and Z. GhahramaniЃн, **"Learning from labeled and unlabeled data with label propagation",** 2002.

[15] 15. S. Mirjalili, S. M. Mirjalili, and A. Lewis, **"Grey wolf optimizer,"** *Advances in engineering software*, vol. 69, pp. 46-61, 2014.

[16] Newman, M.E. and M. Girvan, **"Finding and evaluating community structure in networks".** *Physical review* E, 200۴. 69(2): p. 026113.

[17] Lusseau D. **"The emergent properties of a dolphin social network"**[J]. *Proceedings of the Royal Society of London. Series B: Biological Sciences*, 2003, 270(Suppl 2): S186- S188.

[18] A. Mohammadzadeh, et al., **"Presenting an improved gray wolf optimization algorithm for Workflow scheduling in cloud computing environment",** *Scientific Research Journal of Soft Computing and Information Technology*, Vol. 8, No. 4, 2018

[19] Jian Zhou, Yuxin Chen, **"Hybridizing five neural-metaheuristic paradigms to predict the pillar stress in bord and pillar method",** *Frontiers in PublicHealth*, 2023,

[20] Maliheh Ghasemzadeh, Mohsen Ashourian, "**Identifying Communities on Static Social Networks"**، *Majlesi Journal of Telecommunication Devices*، Vol. 8, No. 3, September 2019.

Planar Parasitic Monopole Antenna with a Circular Ground Plane for UWB Utility

Motahhare Farrokhfar[1], Seyyed Ali Hosseini[2], Mohammad Hossein Farrokhfar[3]
1- IRAN Meteorological Organization, Tehran, Iran
Email: m.farrokhfar67@gmail.com (Corresponding author)
2- Faculty of Technical and Engineering, Imam Hossein University, Tehran, Iran
Email: hosseini1364@gmail.com
3- Department of Electrical Engineering, Technical and Vocational University (TVU), Tehran, Iran
Email: Hfarrokhfar@gmail.com

ABSTRACT:
This paper proposes a monopole antenna with two-pair sleeves that is fed through a coplanar waveguide. The new structure is composed of a triangular radiator and sleeves in size of 40× 40×1.6 mm3. The suggested structure is constructed on an FR-4 PCB layer with a dielectric constant of ε r=4.3. The best results are obtained by parameters sweep study with the CST simulator. According to the results, the bandwidth range is 2.45-11 GHz, expressing that the compact design covers an ultrawide bandwidth. The optimized antenna is manufactured and the measurement outcome of the return loss is compared with the CST simulator results at various frequencies, representing a satisfactory consistency of simulation and measurement results.

KEYWORDS: Sleeve Antenna, Triangular Monopole, Coplanar Waveguide-Fed, Ultra-Wideband.

1. INTRODUCTION

Combining the traditional Ultra-wideband (UWB) antennas with modern integrated systems is not feasible due to the complicated systems and big dimensions. The low-profile planar antennas are a favorite in UWB applications. Therefore, the surface antennas are taken into consideration when they are fed by a coplanar waveguide based on their significant competencies e.g., broadband frequency ranges, compact size, simple matching with integrated circuits, and stable radiation patterns. Several structures of the monopole antenna have been studied in wideband applications including circular, square, elliptical, trapezoidal, rectangular, and mixed-shape structures [1]-[7]. Various approaches have been suggested to improve the antenna bandwidth. Printing parasitic elements around the main monopole antenna can increase the bandwidth of the planar antenna [8]-[12]. The triangular monopole antenna in previous studies had a good impedance bandwidth but needs to be enhanced to achieve better performance [13]-[14]. Another way to improve the antenna bandwidth is to shape the ground plane. In [16], the slots are cut from the circular monopole antenna and ground plane. A trapezoid monopole antenna with a sleeve and slots embedded in the ground plate to increase the bandwidth was presented in [17].

This work introduces a new triangular radiator with two-pair sleeves ranging from 2.45-11 GHz. Finally, the ground plane of the suggested antenna is modified circularly.

2. ANTENNA STRUCTURE

Fig. 1 presents the suggested antenna. As shown, the ground plate is truncated and parasitic elements are extensions of ground planes as sleeves. The substrate is FR-4 with ε_r=4.3. The two-pair sleeves are parallel to the monopole radiator and have grown out of the ground plane. The printed-strip sleeve lengths and spacing are denoted as L_{S1}, L_{S2}, $W_{S1,}$ and W_{S2}, respectively. The variables include the monopole height (h_m), sleeves lengths (L_{S1}, L_{S2}), monopole, sleeves flare angle (θ), sleeves widths (W_{S1}, W_{S2}), and spacing between the sleeves and the monopole (S_1, S_2).

Paper type: Research paper
Received: 16 November 2023; revised: 22 December 2023; accepted: 19 January 2024; published: 1 March 2024
How to cite this paper: M. Farrokhfar, S. A. Hosseini, and M. H. Farrokhfar, **"Planar Parasitic Monopole Antenna with a Circular Ground Plane for UWB Utility"**, *Majlesi Journal of Telecommunication Devices*, Vol. 13, No. 1, pp. 17-25, 2024.

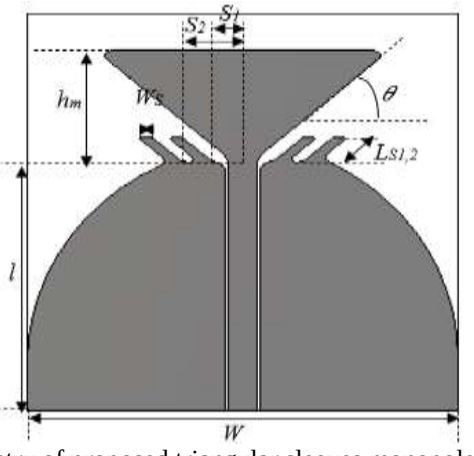

Fig. 1. Geometry of proposed triangular sleeves monopole antenna.

3. ANALYSIS AND SIMULATION

The appropriate structure of the antenna is designed and simulated with the genetic algorithm (GA) optimizer at the CST simulator. The aim of the optimization process was to determine the antenna dimensions which resulted in a return loss of less than -10dB. The GA is a method of random search; thus, it is not accurate. Therefore, the results of the model were improved by Sweep parameters. The strip and gap width are set to 2.6 mm and 0.28 mm respectively to reach the 50ohm CPW feed. The optimal selected parameters are shown in Table 1.

Table 1. The best parameters of the antenna.

parameters	Value(mm)
h_m	10.8
L_S	2.8
W_S	1.3
l	25
S_1	1.2
S_2	4
θ	0.72(rad)
W	40

As displayed in Fig. 2, the antenna bandwidth is 2.5-5.1 GHz without the sleeves, which denotes a relatively small bandwidth. Through adding two-pair sleeves to the printed triangular radiator, the bandwidth is improved, covering the 2.5-7.5 GHz range (return loss ≤ -10 dB), however, two-pair sleeves sound more efficient because of the wide impedance bandwidth from 2.45 to 11 GHz. Furthermore, we study three pair sleeves surrounding the monopole antenna, which leads to increased antenna size, without improving the bandwidth.

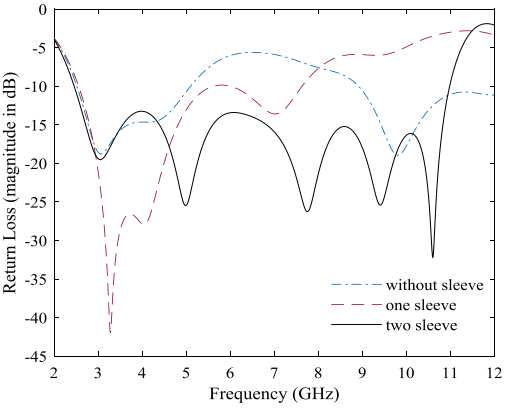

Fig. 2. The results of the simulation of the S_{11} of the designed antenna without the sleeve, with one and two-pair sleeves.

4. PARAMETRIC STUDY AND DISCUSSION

Fig. 3 shows the simulations of the current distributions from the suggested structure at the frequencies of 5.5, 7.5, and 9.5 GHz respectively. It represents a strong current distribution around the sleeves and curved ground.

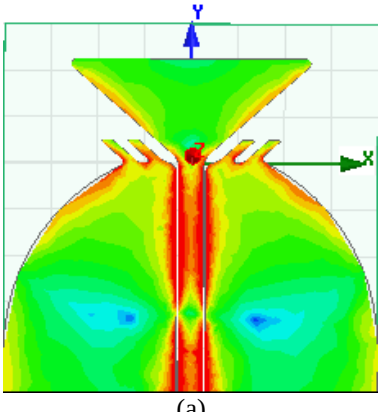

(a)

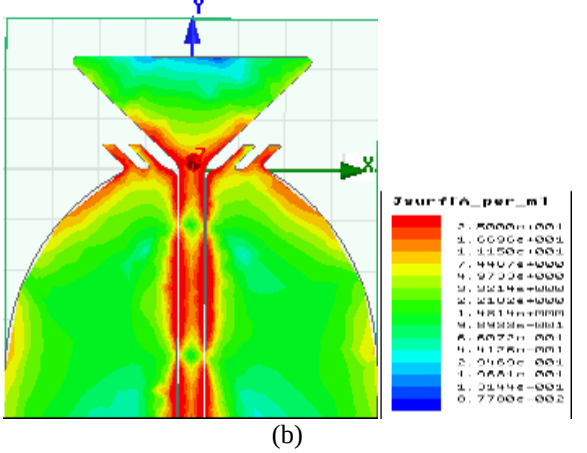

(b)

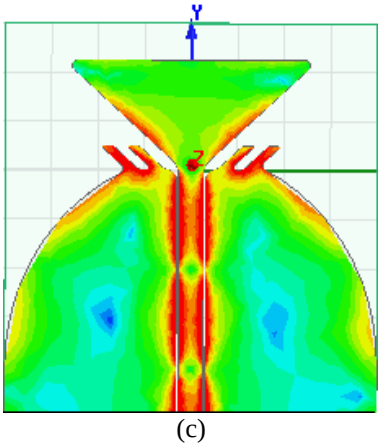

(c)

Fig. 3. Simulation of the current distributions for the suggested structure at, a) 5.5 GHz, b) 7.5 GHz, c) 9.5 GHz.

Fig. 4 presents the effect of flare angle (θ) on the return loss. It is a main parameter at the return loss of the structure. The optimum return loss for flare angle is about θ =0.72 rad.

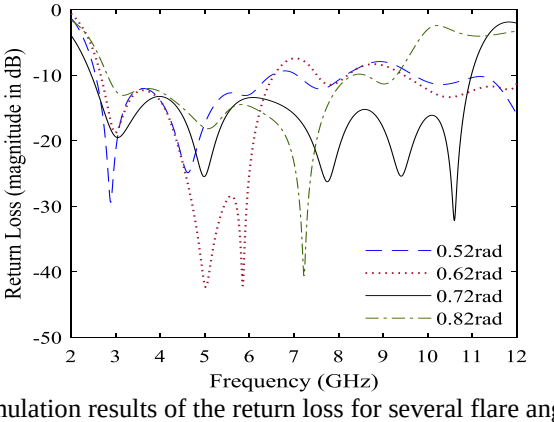

Fig. 4. Simulation results of the return loss for several flare angles (θ).

The return loss curves shown in Fig. 5 are derived through simulations of various monopole heights. The monopole height affects lower frequencies of bandwidth. The optimum return loss is about h_m=10.8 mm for monopole height.

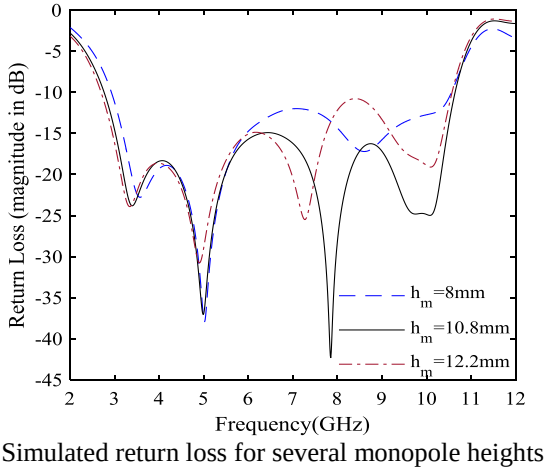

Fig. 5. Simulated return loss for several monopole heights (h_m).

The spacing between sleeves and the main radiator effect the higher frequency of bandwidth, as shown in Fig. 6. The best results are obtained for S_1 (spacing between the main radiator and the near sleeve) = 1.2 mm and S_2 (spacing between the main radiator and farther sleeve) = 4 mm.

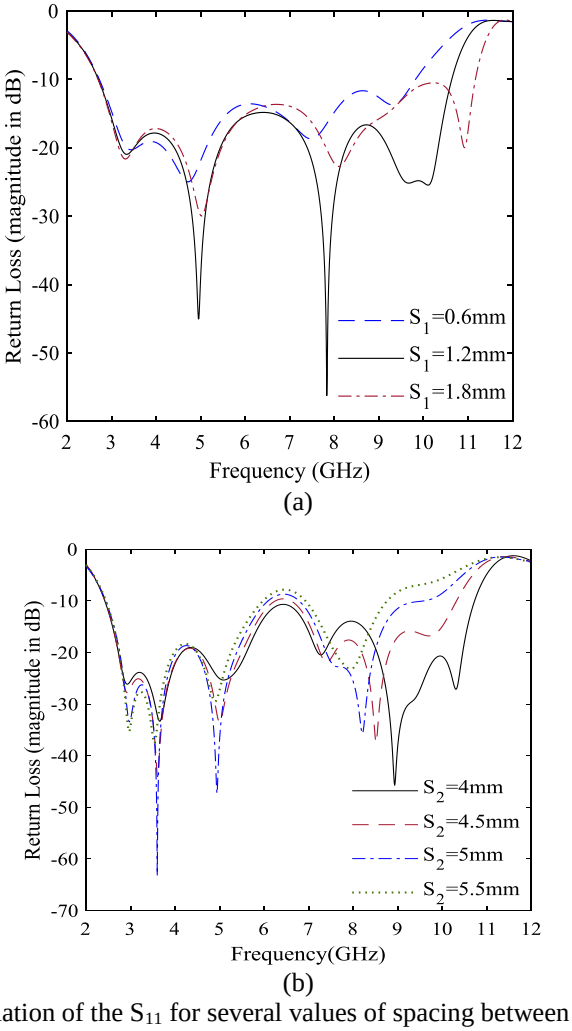

Fig. 6. The results of the simulation of the S_{11} for several values of spacing between the main radiator and sleeves; a) the near sleeves (S_1), b) the farther sleeves (S_2).

Fig. 7 illustrates the simulation of the return loss for several sleeve-length L_S. The sleeve length affects all over the bandwidth, as observed. L_S=2.8 mm has the best bandwidth.

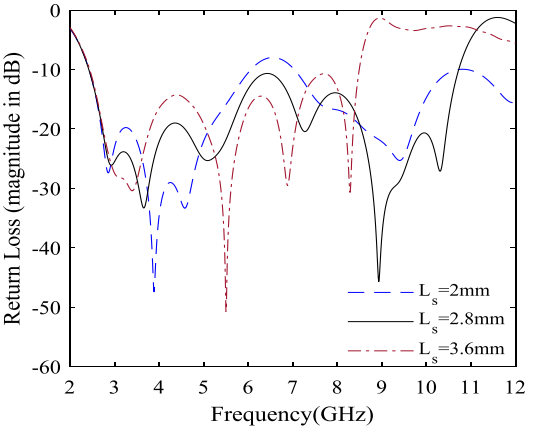

Fig. 7. The Simulation results of the S_{11} for several values of sleeves length (L_s).

The simulation results of the S_{11} for various amounts of sleeve width are plotted in Fig. 8. All of the values control good bandwidth, but W_S =1.3mm holds the better result.

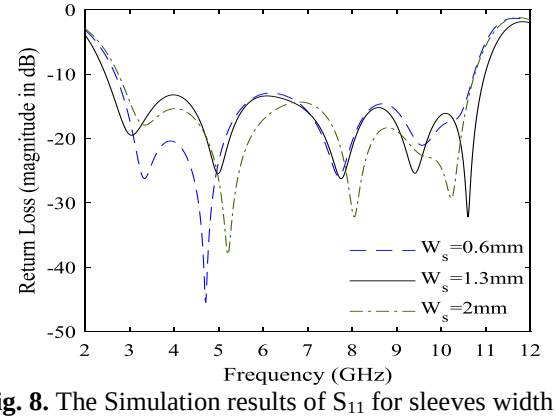

Fig. 8. The Simulation results of S_{11} for sleeves width (W_S).

Fig. 9 displays the peak gain of the suggested sleeve structure. The peak gain is almost 6.8 dBi at 10.7 GHz frequency.

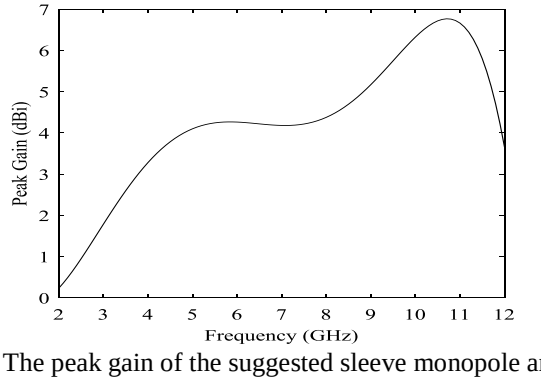

Fig. 9. The peak gain of the suggested sleeve monopole antenna.

5. FABRICATION AND MEASUREMENTS

An experimental evaluation of the optimized antenna was conducted by implementing and testing the proposed antenna. For this purpose, the printed sleeves monopole antenna is manufactured on an FR-4 PCB substrate. Fig. 10 shows the manufactured proposed antenna.

Fig. 10. The manufactured sleeves monopole antenna.

The return loss curves of the measuring and simulation results of the designed structure are plotted in Fig. 11. The 10-dB bandwidth reaches 2.45 - 11 GHz to meet the requirements of the UWB application. According to equations 1 and 2, the bandwidth efficiency is 127.14%.

$$BW(\%) = \frac{f_H - f_L}{f_C} \quad (1)$$

$$f_C = \frac{f_H + f_L}{2} \quad (2)$$

Where f_H, f_L, f_C are the operation band's upper, lower, and center frequency, respectively. The simulation corresponds to measurement fairly.

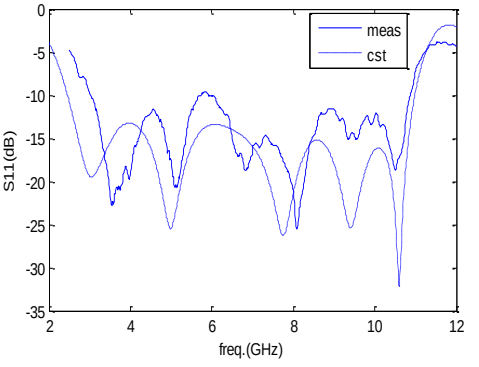

Fig. 11. Results of simulation and measuring of return loss.

The radiation profiles measured in the x-y E and H planes at 5.5 GHz are shown in Fig. 12.

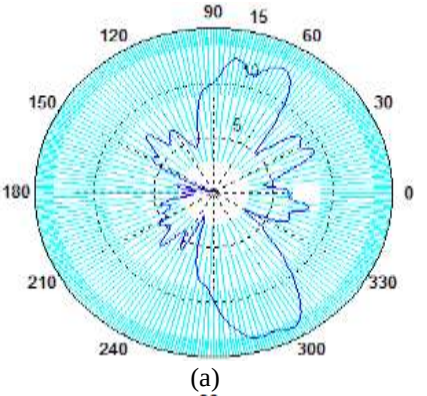

(a)

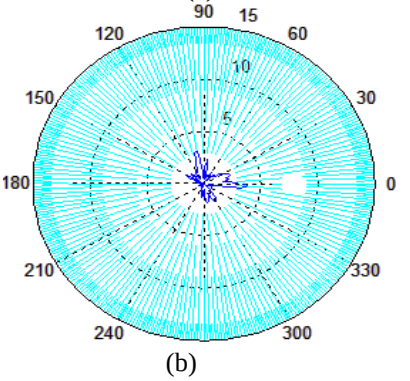

(b)

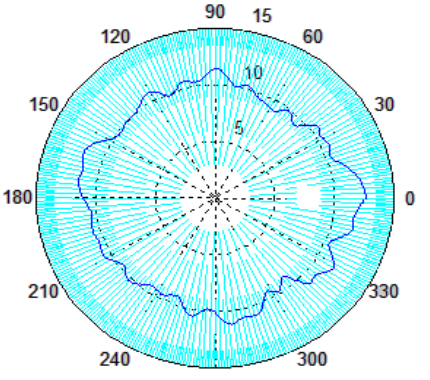

(c)

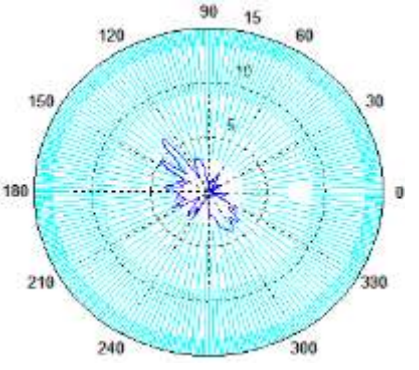

(d)

Fig. 12. The measuring results of the radiation patterns from the designed structure at 5.5 GHz; a) Co polarization in E-Plane, b) Cross polarization in E-Plane, c) Co polarization in H-Plane, d) Cross polarization in H-Plane.

Finally, a comparison proposed antenna with recent monopole antennas are in Table 2. This table verifies the improvement in the bandwidth of our proposed antenna.

Table 2. Comparison between monopole antennas

Reference	Frequency range (GHz)	Bandwidth (%)	Dimensions (mm^3)
[18]	0.24-0.95	119.3	30×30×320
[19]	3.92-7.52	62.94	30×32×1.6
[20]	2.87-11.44	119.7	22×18×1.6
[21]	0.47-0.9	63	185×45×1.6
[22]	0.2-0.51	86	530×150×50
[23]	2.4-7.6	104	40.5×30.5×1.6
Proposed antenna	2.45-11	127.14	40×40×1.6

6. CONCLUSION

The printed sleeve triangular monopole antenna was proposed. The CPW-fed characteristics, circular ground plane, and loading two-pair sleeves are tuned to the input impedance matching. The low profile of the designed structure is appropriate for integrated systems. The proposed structure has achieved an ultra-wide bandwidth. The accuracy of the

result has been verified by the agreement between the simulation and measurement results. Also, the measurement results of the radiation patterns of the designed structure show the omnidirectional antenna. This design is a potential alternative for future UWB devices based on the results.

REFERENCES

[1] Y. W. Y. Z. a. H. Z. S. Hu, **"Design of a CPW-Fed Ultra-Wide Band Antenna,"** *Open Journal of Antennas and Propagation*, vol. 1, no. 2, pp. 18-22, Sep. 2013.

[2] G. K. K. R. N.P. Agrawall, **"Wide-band Planar Monopole Antennas,"** *IEEE Trans. Antennas Propag*., vol. 46, no. 2, pp. 294-295, Feb. 1998.

[3] M. C. F. M. F. B. A. V. N. E. A. Daviu, **"Wideband Double-fed Planar Monopole Antennas,"** *Electron*. Lett., vol. 39, no. 23, pp. 1635-1636, Nov. 2003.

[4] H. Chen, H.M. Chen and W.S. Chen, **"Planar CPW-fed sleeve monopole antenna for ultra-wideband operation,"** *IEE PROCEEDINGS MICROWAVES ANTENNAS AND PROPAGATION*, vol. 152, no. 6, p. 491, Dec. 2005.

[5] H. Chen, **"Compact broadband microstrip-line-fed sleeve monopole antenna for DTV application and ground plane effect,"** *IEEE Antennas and Wireless Propagation Letters*, vol. 7, pp. 497-500, Aug. 2008.

[6] P. Ramanujam, P. R. Venkatesan, Ch. Arumugam and M. Ponnusamy, **"Design of miniaturized super wideband printed monopole antenna operating from 0.7 to 18.5 GHz,"** *AEU-International Journal of Electronics and Communications*, vol. 123, p. 153273, 2020.

[7] B. Bag, S. Biswas and P. P. Sarkar, **"A wide circularly polarized dual- band isosceles trapezoidal monopole antenna with modified ground plane,"** *International Journal of Communication Systems*, vol. 35, no. 3, p. 5037, 2022.

[8] M. Rahman, M. A. Stuchly and M. Okoniewski, **"Dual-Band Strip-Sleeve Monopole for Handheld Telephone,"** *Microwave Opt. Technol. Lett.*, vol. 21, no. 2, pp. 79-82, Apr. 1999.

[9] H. D. Chen, H. M. Chen and W.-S. Chen, **"Planar CPW-fed Sleeve Monopole Antenna for Ultra-Wideband Operation,"** *IEE Proc.-Microw. Antenna Porpaga.*, vol. 152, no. 6, pp. 491-494, Dec. 2005.

[10] S. B. Chen, Y. C. Jioa, W. Wang, and Q.-Z. Liu, **"Wideband CPW-fed Unipla-nar Sleeveshaped Monopole Antenna,"** *Microwave Opt. Technol. Lett*., vol. 47, no. 3, pp. 245-247, Nov. 2005.

[11] N. G, D.S, and U. S, **"Sleeve Monopole Antenna for WiMAX Applications,"** *India Conference (INDICON)*, 2012 Annual IEEE., pp. 588-591, 2012.

[12] Y. Zimu, L. Jiangang, Z. Dailiang, and Y. Aishuai, **"Compact Monopole Sleeve Antenna Reaches 11.8 GHz,"** *Microwaves & RF*., vol. 51, no. 7, Jul. 2012.

[13] G. Brown and O.M. Woodward, **"Experimentally Determined Radiation Characteristics of Conical and Triangular Antennas,"** *RCA Rev*., vol. 13, no. 4, pp. 425-452, Dec. 1952.

[14] K. L. Wong and Y. F. Lin, **"Stripline-fed Printed Triangular Monopole,"** *Electron. Lett*., vol. 33, pp. 1428-1429, Aug. 1997.

[15] C.-C. Lin, K.-Y. Kan and H.-R. Chuang, **"A 3-8-GHz Broadband Planar Triangular Sleeve Monopole Antenna for UWB Communication,"** *in Proc. IEEE Antennas Propagat. Society International Symposium*, pp. 5741-5744, June 2007.

[16] A. De, B. Roy and A. K. Bhattacharjee, **"Design and investigations on a compact, UWB, monopole antenna with reconfigurable band notches for 5.2/5.8 GHz WLAN and 5.5 GHz Wi- MAX bands,"** *International Journal of communication systems*, vol. 33, no. 7, p. 4323, 2020.

[17] B. Bag, S. Biswas and P.P. Sarkar, **"A wide circularly polarized dual- band isosceles trapezoidal monopole antenna with the modified ground plane,"** *International Journal of Communication Systems*, vol. 35, no. 3, p. 5037, 2022.

[18] X. H. Zhang, X. W. Dai, W. Sun, H. Jin and G. Q. Luo, **"Sleeve monopole antenna with choke structure for broadband application,"** *IEEE Antennas and Wireless Propagation Letters*, vol. 20, no. 7, pp. 1230-1233, 2021.

[19] M. Midya, Sh. Bhattacharjee and M. Mitra, **"Broadband circularly polarized planar monopole antenna with G-shaped parasitic strip,"** *IEEE Antennas and Wireless Propagation Letters*, vol. 18, no. 4, pp. 581-585, 2019.

[20] T. Gayatri, N. Anveshkumar and V. K. Sharma, **"A compact planar UWB antenna for spectrum sensing in cognitive radio,"** *In 2020 International Conference on Emerging Trends in Information Technology and Engineering (ic-ETITE) IEEE*, pp. 1-5, 2020.

[21] J. Owusu, M. R. B. Hamid, S. T.-Koduah and S. Afoakwa, **"Omnidirectional antenna with modified ground plane for wideband DVB in handheld devices,"** *Scientific African*, vol. 13, p. e00872, 2021.

[22] D. Qin and B. Sun, **"VHF/UHF wideband slim monopole antenna with distributed matching structures,"** *International Journal of Antennas and Propagation 2022*, 2022.

[23] A. P. Acharya, T. K. Das, and T. Shaw, **"Design and analysis of compact flower-shaped wideband slotted monopole antenna for RFID reader applications,"** *AEU-International Journal of Electronics and Communications*, vol. 169, p. 154718, 2023.

A Comparative Analysis of Digital Audio Encoders: LPC, CELP, and MELP, Evaluating Quality and Complexity of Transmitted Content

Saeed Talati[1], Pouriya Etezadifar[2], Mohammad Reza Hassani Ahangar[3], Mahdi Molazade[4]

1- PhD Candidate, Faculty of Electrical Engineering Department, Imam Hossein University, Tehran, Iran.
Email: Saeed.Talati@ihu.ac.ir

2- Assistant Professor, Faculty of Electrical Engineering Department, Imam Hossein University, Tehran, Iran.
Email: petezadifar@ihu.ac.ir (Corresponding Author)

3- Professor, Faculty of Electrical Engineering Department, Imam Hossein University, Tehran, Iran.
Email: MRHassani@ihu.ac.ir

4- Assistant Professor, Faculty of Electrical Engineering Department, Imam Hossein University, Tehran, Iran.
Email: mmollazade@ihu.ac.ir

ABSTRACT:
This article compares the quality and complexity of LPC, CELP, and MELP standard audio encoders. These standards are based on linear predictive and are used in sound (speech) processing. These standards are powerful high-quality speech coding methods that provide highly accurate estimates of audio parameters and are widely used in the commercial (mobile) and military (NATO) communications industries. To compare LPC, CELP, and MELP audio encoders in two male and female voice modes and four voice models: quiet, Audio recorded without sound by the microphone, MCE, office, and two noise models 1% and 05% were used. The simulation results show the complexity of MELP is higher than LPC and CELP in terms of both processor and memory requirements. The MELP analyzer requires 72% of its total processing time. This additional memory is, due to the vector quantization tables MELP uses for the linear spectral frequencies (LSFs) and the Fourier magnitude. Also, According to the quality comparison test using the MOS index, MELP has the highest score, followed by CELP and LPC.
.

KEYWORDS: Quality, Complexity, LPC, CELP, MELP.

1. INTRODUCTION

In 1966, Linear Predictive Coding (LPC) was presented and in 1978 this method was completed [1]. LPC is one of the most common audio coding methods that converts analog audio to digital at 2400 bps.

LPC is one of the powerful methods of high-quality audio encoder analysis that provides very accurate estimates of audio parameters. The way LPC works is that speech-like audio signals are produced by a noise, and sounds with frequencies have successively added to them alternately. This method is the closest approximation to the real sound.

The Code Excited Linear Predictive (CELP) was presented in 1985 [2]. CELP is a linear speech encoder programming algorithm that converts analog audio to digital audio at 4800 bits per second. This method is high quality and is used in MPEG-4 audio speech encoder.

The Mixed Excitation Linear Predictive (MELP) was registered in 1995 based on LPC. This audio speech coder was standardized in 1997[3]. This method is one of the most common audio encoding methods that converts analog audio to digital at 2400 bits per second. This method is mainly used in military applications and satellite communications, secure voice transmission, and the safety of radio communications.

Paper type: Research paper
Received: 7 November 2023; revised: 15 December 2023; accepted: 28 January 2024; published: 1 March 2024
How to cite this paper: S. Talati, P. Etezadifar, M. R. Hassani Ahangar, M. Molazade, **"A Comparative Analysis of Digital Audio Encoders: LPC, CELP, and MELP, Evaluating Quality and Complexity of Transmitted Content"**, *Majlesi Journal of Telecommunication Devices*, Vol. 13, No. 1, pp. 27-35, 2024.

2. LPC

The working method of LPC is that sound signals similar to speech are produced by noise and sounds with alternating frequencies are successively added to it. This method is the closest approximation to the real sound. LPC analyzes the speech signal by estimating the forms, removing their effects from the speech signal, and estimating the intensity and frequency of the residual noise. The process of eliminating these forms is called inverse filtering, and the remaining signal after subtracting the filtered modeled signal is called the remaining signal. Since the speech signals are different, this process is done in short pieces of the speech signal, which are called frames. In general, LPC compresses the speech signal at 30 to 50 frames per second.

Because LPC is often used to transmit spectrum information, it must be tolerant of transmission errors. Transferring the filter coefficients directly is undesirable because they are very sensitive to error.

In other words, a very small error can change the entire spectrum

2.1. Bit Allocation

Bit allocation of LPC frame should be according to the following table [4].

Table 1. Bit Allocation of LPC Encoder.

Bit	Voiced	Unvoiced	Bit	Voiced	Unvoiced	Bit	Voiced	Unvoiced
1	RC (l)-0	RC(l)-0	19	RC(3)-3	RC(3)-3	37	RC(8)-1	R-6*
2	RC(2)-0	RC(2)-0	20	RC(4)-2	RC(4)-2	38	RC(5)-1	RC(1)-6*
3	RC(3)-0	RC(3)-0	21	R-3	R-3	39	RC(6)-1	RC(2)-6*
4	P1-0	P-0	22	RC(l)-4	RC(l)-4	40	RC(7)-2	RC(3)-7*
5	R2-0	R-0	23	RC(2)-3	RC(2)-3	41	RC(9)-0	RC(4)-6*
6	RC(l)-1	RC(l)-1	24	RC(3)-4	RC(3)-4	42	P-5	P-5
7	RC(2)-1	RC(2)-1	25	RC(4)-3	RC(4)-3	43	RC(5)-2	RC(1)-7*
8	RC(3)-1	RC(3)-1	26	R-4	R-4	44	RC(6)-2	RC(2)-7*
9	P-1	P-1	27	P-3	P-3	45	RC(10)-1	Unused
10	R-1	R-1	28	RC(2)-4	RC(2)-4	46	RC(8)-2	R-7*
11	RC(l)-2	RC(l)-2	29	RC(7)-0	RC(3)-5*3	47	P-6	P-6
12	RC(4)-0	RC(4)-0	30	RC(8)-0	R-5*	48	RC(9)-1	RC(4)-7*
13	RC(3)-2	RC(3)-2	31	P-4	P-4	49	RC(5)-3	RC(1)-8*
14	R-2	R-2	32	RC(4)-4	RC(4)-4	50	RC(6)-3	RC(2)-8*
15	P-2	P-2	33	RC(5)-0	RC(1)-5*	51	RC(7)-3	RC(3)-8*
16	RC(4)-1	RC(4)-1	34	RC(6)-0	RC(2)-5*	52	RC(9)-2	RC(4)-8*
17	RC(1)-3	RC(1)-3	35	RC(7)-1	RC(3)-6*	53	RC(8)-3	R-3*
18	RC(2)-2	RC(2)-2	36	RC(10)-0	RC(4)-5*	54	Synch.	Synch.

3. CELP

CELP is essentially Analysis with Synthesis (AbS) meaning that coding (analysis) is performed with perceptual optimization of the decoded signal (synthesis) in a closed loop, the high complexity of CELP was initially an impractical proposition. However, many ways to speed up the coding process have been found and CELP has become a practical reality [5].

1 P = Pitch
2 R = RMS Amplitude
3 * = Error Control Bit
Bit 0 = least significant bit of data

3.1. Bit Allocation

Bit allocation of CELP frame should be according to the following table [4].

Table 2. Bit Allocation of CELP Encoder.

Bit	Description	Bit	Description	Bit	Description	Bit	Description	Bit	Description	Bit	Description
1	PG(4)-4[4]	25	PG(3)-1	49	LSP 1-2	73	PD(l)-4	97	PG(l)-2	121	LSP 7-2
2	PD(3)-4[5]	26	PD(4)-5	50	PG(3)-2	74	CG(3)-2	98	CG(3)-4	122	CI(4)-2
3	LSP 1-1[6]	27	CG(l)-3	51	HP-1	75	LSP 7-1	99	LSP 10-2	123	PD(l)-1
4	CG(2)-4[7]	28	CI(3)-5	52	PD(3)-1	76	CI(2)-7	100	CI(4)-5	124	PG(2)-4
5	CI(3)-3[8]	29	LSP 7-O	53	CG(4)-3	77	CI(3)-O	101	CI(2)-O	125	CG(3)-3
6	CI(l)-8	30	CI(2)-1	54	LSP 8-1	78	PD(2)-5	102	PD(l)-2	126	LSP 3-1
7	PD(4)-O	31	PD(3)-7	55	PG(3)-O	79	LSP 4-1	103	LSP 5-1	127	CI(l)-7
8	LSP 8-O	32	CI(l)-O	56	CI(2)-8	80	CG(l)-O	104	SP-O[9]	128	PD(3)-2
9	PG(2)-3	33	PG(4)-O	57	PD(4)-1	81	PG(4)-3	105	PG(4)-2	129	CI(2)-6
10	CG(3)-O	34	LSP 4-3	58	CI(4)-O	82	LSP 9-1	106	CG(2)-3	130	LSP 9-2
11	PD(l)-5	35	CG(3)-1	59	LSP 3-2	83	PD(3)-6	107	LSP 2-1	131	PG(4)-1
12	LSP 3-3	36	CI(l)-5	60	PG(2)-O	84	CI(l)-4	108	PD(4)-4	132	CG(l)-1
13	CI(2)-3	37	PD(2)-O	61	PD(l)-6	85	CG(2)-1	109	CI(l)-2	133	PD(2)-4
14	CI(4)-4	38	CI(4)-1	62	CG(2)-O	86	LSP 6-2	110	PG(2)-1	134	HP-3
15	PD(2)-1	39	LSP 9-O	63	CI(3)-6	87	CI(4)-3	111	CI(3)-7	135	LSP 6-O
16	LSP 10-0	40	CI(3)-8	64	LSP 10-1	88	PG(2)-2	112	LSP 4-O	136	PG(3)-3
17	PG(l)-3	41	PG(l)-4	65	PG(l)-1	89	PD(4)-3	113	CI(2)-5	137	CI(4)-6
18	CG(4)-O	42	CG(2)-2	66	CI(4)-7	90	LSP 1-0	114	PD(l)-7	138	PD(l)-O
19	LSP 5-2	43	PD(l)-3	67	PD(3)-3	91	CG(4)-2	115	PG(l)-O	139	LSP 2-3
20	PD(3)-O	44	LSP 6-1	68	CG(l)-2	92	LSP 8-2	116	CG(4)-4	140	CG(4)-1
21	HP-O[10]	45	CI(3)-4	69	LSP 5-3	93	CI(2)-4	117	LSP 5-O	141	CI(3)-2
22	CI(l)-1	46	CI(2)-2	70	CI(l)-6	94	HP-2	118	PD(4)-2	142	LSP 4-2
23	CI(4)-8	47	CG(l)-4	71	LSP 2-O	95	PD(2)-2	119	CI(l)-3	143	PD(3)-5
24	LSP 2-2	48	PD(2)-3	72	PG(3)-4	96	LSP 3-O	120	CI(3)-1	144	SY[11]

4 PG(n)-i = Adaptive Code Gain
5 PD(n)-i = Adaptive Code Index
6 LSP j-i = Line Spectral Parameter (LSP),
where j = LSP number
7 CG(n)-i = Fixed, Stochastically-derived Code Gain
8 CI(n)-i = Fixed, Stochastically-derived Code Index
9 SP = Expansion Bit
10 HP-i = Parity
11 SY = Synchronization Bit
Note: i = bit number, with O being the least significant bit
n = subframe number

Paper type: Research paper
https://doi.org/10.30486/mjee.2023.1979949.1074
Received: 5 October 2023; revised: 28 November 2023; accepted: 13 December 2023; published: 1 March 2024
How to cite this paper: Gh. Hematipour, S. A. Sadatnoori, S. A. Seyedkavoosi, **"Digital Sigma-Delta Modulator with Effective Random Dither and without Unwanted Tones"**, *Majlesi Journal of Telecommunication Devices*, Vol. 13, No. 1, pp. 9-12, 2024.

4. MELP

MELP is based on the traditional LPC model and uses additional features such as mixed excitation, non-periodic pulses, adaptive spectrum enhancement, pulse dispersion filter, and Fourier magnitude modeling to improve performance. Adding these features allows the encoder to better match the features of the input speech. [6].

4.1. Bit Allocation

Bit allocation of MELP frame should be according to the following table [6].

Table 3. Bit Allocation of MELP Encoder.

Bit	Voiced	Unvoiced	Bit	Voiced	Unvoiced	Bit	Voiced	Unvoiced
1	G12(2)-1	G(2)-1	19	LSF(1)-7	LSF(1)-7	37	G(1)-1	G(1)-1
2	BP14-1	FEC13(1)-1	20	LSF(4)-6	LSF(4)-6	38	BP-3	FEC(1)-3
3	P15-1	P-1	21	P-4	P-4	39	BP-2	FEC(1)-2
4	LSF16(2)-1	LSF(2)-1	22	LSF(1)-6	LSF(1)-6	40	LSF(2)-2	LSF(2)-2
5	LSF(3)-1	LSF(3)-1	23	LSF(1)-5	LSF(1)-5	41	LSF(3)-4	LSF(3)-4
6	G(2)-4	G(2)-4	24	LSF(2)-6	LSF(2)-6	42	LSF(2)-3	LSF(2)-3
7	G(2)-5	G(2)-5	25	BP-4	FEC(1)-4	43	LSF(3)-3	LSF(3)-3
8	LSF(3)-6	LSF(3)-6	26	LSF(1)-4	LSF(1)-4	44	LSF(3)-2	LSF(3)-2
9	G(2)-2	G(2)-2	27	LSF(1)-3	LSF(1)-3	45	LSF(4)-4	LSF(4)-4
10	G(2)-3	G(2)-3	28	LSF(2)-5	LSF(2)-5	46	LSF(4)-3	LSF(4)-3
11	P-5	P-5	29	LSF(4)-5	LSF(4)-5	47	AF17	FEC(4)-3
12	LSF(3)-5	LSF(3)-5	30	FM18-1	FEC (4)-1	48	LSF(4)-2	LSF(4)-2
13	P-6	P-6	31	LSF(1)-2	LSF(1)-2	49	FM-5	FEC(3)-3
14	P-2	P-2	32	LSF(2)-4	LSF(2)-4	50	FM-4	FEC(3)-2
15	P-3	P-3	33	FM-8	FEC(2)-3	51	FM-3	FEC(3)-1
16	LSF(4)-1	LSF(4)-1	34	FM-7	FEC(2)-2	52	FM-2	FEC(4)-2
17	P-7	P-7	35	FM-6	FEC(2)-1	53	G(1)-3	G(1)-3
18	LSF(1)-1	LSF(1)-1	36	G(1)-2	G(1)-2	54	SYNC	SYNC

5. COMPARISON

Audio encoder standards LPC, CELP, and MELP were thoroughly reviewed. It is necessary to compare their performance in terms of quality, Intelligibility, Communicability, Recognizability, and complexity for two different types of speech (male and female) in order to conclude which one performs better.

5.1. Quality

For quality testing, we use MOS[19] for benign noise conditions [7]. Quality testing is often used to supplement or replace comprehensibility testing. It provides a picture of the listeners' personal opinions about the signal sent by the communication systems or processed by the algorithms under test.

MOS test has been done in four audio noise conditions and two-channel conditions. The two error environments

12 Gain
13 Forward Error Correction Parity Bits
14 Band pass Voicing
15 Pitch voicing
16 Line Spectral Frequencies
17 Aperiodic Flag
18 Fourier Magnitude
Note: Bit 1 = least significant bit of data set
19 Mean Opinion Score

tested are: a 1% random bit error channel and a 0.5% random block error channel. Block error contains 50% error in a 35 ms block. Q-H250 is Audio recorded without sound by the microphone

"MCE" is a mobile command environment. The office is recorded in a modem office. Quiet is a soundless environment [8].

The MOS test results for LPC, CELP, and MELP audio encoders are shown in Figs. 1 to 4.

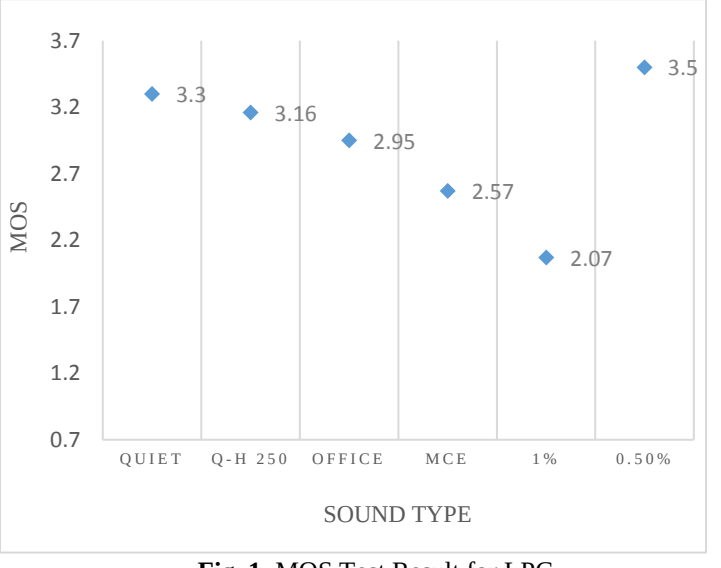

Fig. 1. MOS Test Result for LPC.

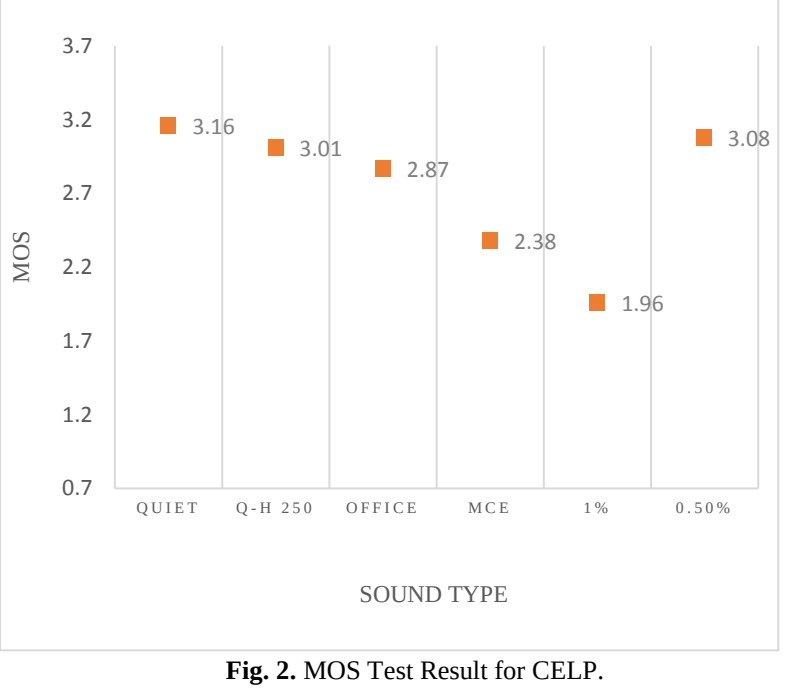

Fig. 2. MOS Test Result for CELP.

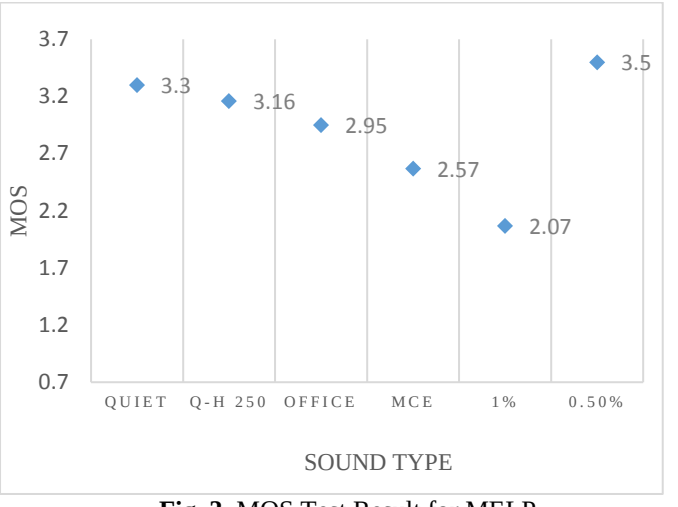

Fig. 3. MOS Test Result for MELP.

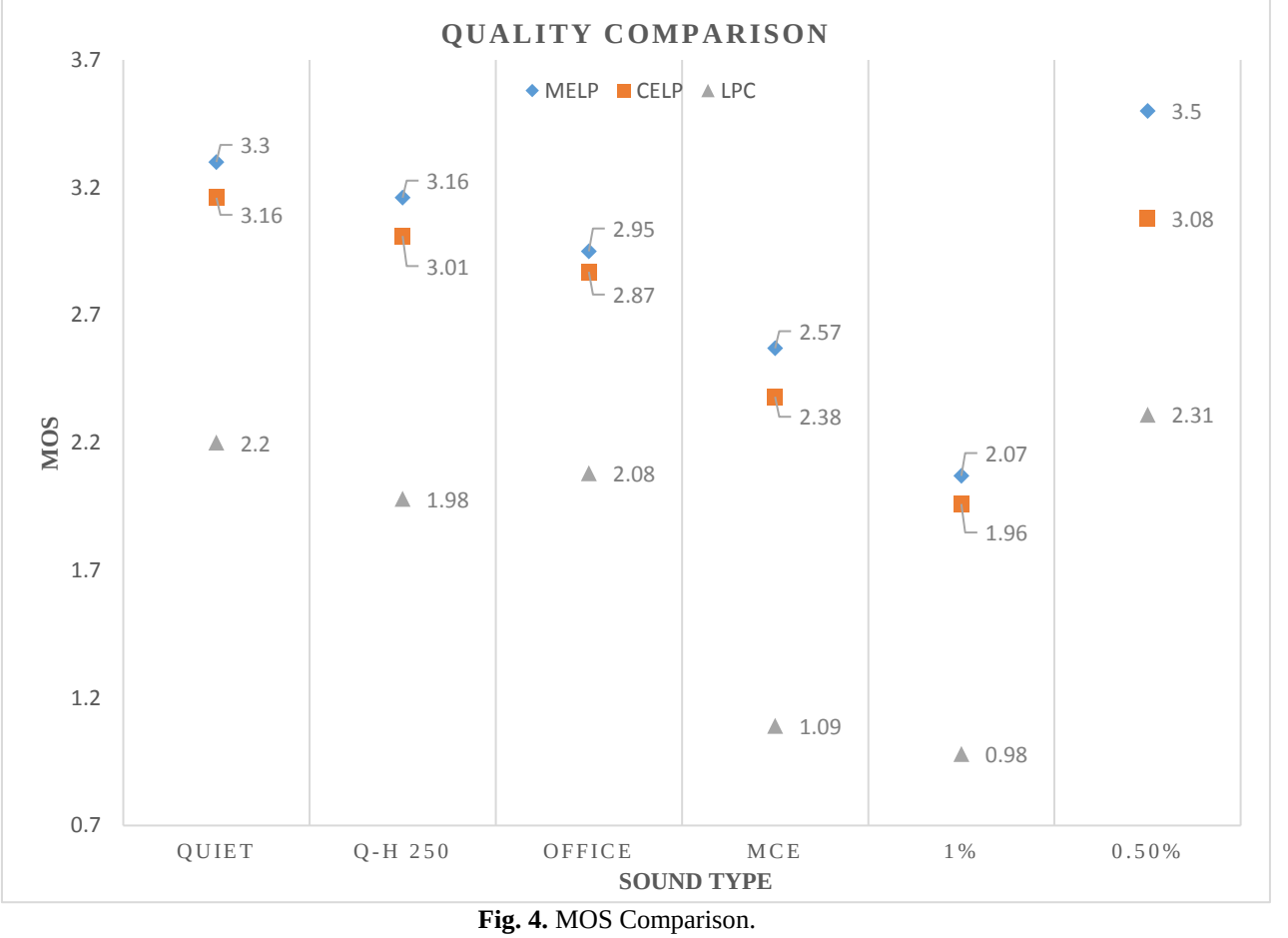

Fig. 4. MOS Comparison.

Relative coder ranking is easily seen in Figure 4. In all environments, MELP shows the highest MOS score, followed by CELP, and LPC.

MELP and LPC coders scored higher overall for male speakers than female speakers. Only in the 0.5% block error condition did the female MELP score exceed the male score, but this variance was within the standard error. The CELP coder, in contrast, scored higher overall for female speakers than for male speakers. This was especially bad in the office

environment. CELP on QH250 also showed significantly higher scores for female speakers [8]. Table 4 shows the simulation results obtained from each of the standards in different modes.

Table 4. MOS simulation results.

Bit	Quiet	Q-H250	Office	MCE	1%	. 5%
MELP	3.30	3.16	2.95	2.57	2.07	3.50
CELP	3.16	3.01	2.87	2.38	1.96	3.08
LPC	2.20	1.98	2.08	1.09	.98	2.31

6. COMPLEXITY

Complexity was measured using MIPS[20], read only memory (ROM) and random access memory (RAM) measurements.

Table 5. Complexity Comparison [8].

Coder	MIPS	RAM	ROM
MELP	20.43	98.2K	128K
CELP	17.0	14.8K	128K
LPC	8.7	12.93K	128K

As Table 5 shows, MELP complexity exceeds, LPC, and CELP in both processor and memory requirements. The MELP analyzer requires 72% of its total processing. These additional memory requirements are due to vector quantization tables which MELP uses for both line spectral frequencies (LSFs) and Fourier magnitudes [8].

7. SUPPORT

Adapted from Saeed Talati's doctoral thesis at comprehensive Imam Hossein University entitled "Recognition of digital audio steganography in LPC10, CELP, and MELP audio encoder standards".

8. CONCLUSION

In this article, Standard audio Encoders LPC, CELP, and MELP are compared in the two areas of quality and complexity. These audio coding techniques are powerful audio coding standards that are widely used in the mobile, commercial and military industries (official NATO standard). The quality comparison test using different sounds is given in figure 4. The obtained results show that MELP has the highest score, followed by CELP and LPC. Quality comparison using the MOS index shows that MELP has the highest score, followed by CELP and LPC. The complexity comparison test using different voices is shown in Table 4. The obtained results show that the complexity of MELP is higher than LPC and CELP in terms of both processor and memory requirements. The MELP analyzer requires 72% of its total processing time. This additional memory is, of course, due to the vector quantization tables that MELP uses for the linear spectral frequencies (LSFs) and the Fourier magnitude.

REFERENCES

[1] Bishnu Atal **"The History of Linear Prediction"**. *ICASSP '78. IEEE Signal Processing Magazine*, vol.23, no2, march 2006. 154-161.

[2] Bishnu Atal and Manfred Schroeder. **"Predictive coding of speech signals and subjective error criteria"**. *ICASSP '78. IEEE International Conference on Acoustics*, Speech, and Signal Processing. 3: 573–576, 1978.

[3] A. V. McCree and T. P. Barnwell, **"A mixed excitation LPC vocoder model for low bit rate speech coding"**. *IEEE Transactions on Speech and Audio Processing*, vol. 3, no. 4, pp. 242-250, July 1995.

[4] J. J. D. van Schalkwyk, D. J. Joubert and J. G. van der Linde, **"Linear predictive speech coding at 2400 b/s,"** *in Transactions of the South African Institute of Electrical Engineers*, vol. 84, no. 3, pp. 146-152, June 1993.

[5] M. Schroeder and B. Atal, **"Code-excited linear prediction (CELP): High-quality speech at very low bit rates,"** *ICASSP '85. IEEE International Conference on Acoustics, Speech, and Signal Processing*, 1985, pp. 937-940, doi: 10.1109/ICASSP.1985.1168147.

[6] Weiran Lin, Soo Ngee Koh and Xiao Lin, **"Mixed excitation linear prediction coding of wideband speech at 8 kbps,"** *2000 IEEE International Conference on Acoustics, Speech, and Signal Processing. Proceedings* (Cat. No.00CH37100), 2000, pp. II1137-II1140 vol.2, doi: 10.1109/ICASSP.2000.859165.

[7] J.D. Tardelli, E.W. Kreamer, **"Vocoder Intelligibility and Quality Test Methods",** *IEEE International Conference on Acoustics, Speech, and Signal Processing*, Atlanta, Georgia, USA, 1996.

20 million instructions per second

[8] M. A. Kohler, **"A comparison of the new 2400 bps MELP Federal Standard with other standard coders,"** *1997 IEEE International Conference on Acoustics, Speech, and Signal Processing*, 1997, pp. 1587-1590 vol.2, doi: 10.1109/ICASSP.1997.596256.

[9] Saeed Talati, Pouriya Etezadifar. (2020). **"Providing an Optimal Way to Increase the Security of Data Transfer Using Watermarking in Digital Audio Signals",** *MJTD*, vol. 10, no. 1.

[10] Hashemi, Seyed & Barati, Shahrokh & Talati, S. & Noori, H. (2016). **"A genetic algorithm approach to optimal placement of switching and protective equipment on a distribution network".** *Journal of Engineering and Applied Sciences*. 11. 1395-1400.

[11] Hashemi, Seyed & Abyari, M. & Barati, Shahrokh & Tahmasebi, Sanaz & Talati, S. (2016). **"A proposed method to controller parameter soft tuning as accommodation FTC after unknown input observer FDI".** *Journal of Engineering and Applied Sciences*. 11. 2818-2829.

[12] S. Talati, A. Rahmati, and H. Heidari. (2019) **"Investigating the Effect of Voltage Controlled Oscillator Delay on the Stability of Phase Lock Loops",** *MJTD*, vol. 8, no. 2, pp. 57-61.

[13] Talati, S., & Alavi, S. M. (2020). **"Radar Systems Deception using Cross-eye Technique".** *Majlesi Journal of Mechatronic Systems*, 9(3), 19-21.

[14] Saeed Talati, mohamadreza Hasani Ahangar (2020) **"Analysis, Simulation and Optimization of LVQ Neural Network Algorithm and Comparison with SOM"**, *MJTD*, vol. 10, no. 1.

[15] Talati, S., & Hassani Ahangar. M. R. (2020) **"Combining Principal Component Analysis Methods and Self-Organized and Vector Learning Neural Networks for Radar Data",** *Majlesi Journal of Telecommunication Devices*, 9(2), 65-69.

[16] Hassani Ahangar, M. R., Talati, S., Rahmati, A., & Heidari, H. (2020). **"The Use of Electronic Warfare and Information Signaling in Network-based Warfare".** *Majlesi Journal of Telecommunication Devices*, 9(2), 93-97.

[17] Aslinezhad, M., Mahmoudi, O., & Talati, S. (2020). **"Blind Detection of Channel Parameters Using Combination of the Gaussian Elimination and Interleaving".** *Majlesi Journal of Mechatronic Systems*, 9(4), 59-67.

[18] Talati, S., & Amjadi, A. (2020). **"Design and Simulation of a Novel Photonic Crystal Fiber with a Low Dispersion Coefficient in the Terahertz Band".** *Majlesi Journal of Mechatronic Systems*, 9(2), 23-28.

[19] Talati, Saeed, Hassani Ahangar, Mohammad Reza. (2021). **"Radar Data Processing Using a Combination of Principal Component Analysis Methods and Self-Organized and Digitizing Learning Vector Neural Networks",** *Electronic and Cyber Defense*, 9 (2), pp. 1-7.

[20] Talati, S., Alavi, S. M., & Akbarzade, H. (2021). **"Investigating the Ambiguity of Ghosts in Radar and Examining the Diagnosis and Ways to Deal with it"**. *Majlesi Journal of Mechatronic Systems*, 10(2).

[21] Etezadifar, P., & Talati, S. (2021). **"Analysis and Investigation of Disturbance in Radar Systems Using New Techniques of Electronic Attack".** *Majlesi Journal of Telecommunication Devices*, 10(2), 55-59.

[22] Saeed. Talati, Behzad. Ebadi, Houman. Akbarzade **"Determining of the fault location in distribution systems in presence of distributed generation resources using the original post phasors".** QUID 2017, pp. 1806-1812, *Special Issue No.1- ISSN: 1692-343X, Medellín-Colombia*. April 2017.

[23] Talati, Saeed, Akbari Thani, Milad, Hassani Ahangar, Mohammad Reza. (2020). **"Detection of Radar Targets Using GMDH Deep Neural Network"**, *Radar Journal*, 8 (1), pp. 65-74.

[24] Talati, S., Abdollahi, R., Soltaninia, V., & Ayat, M. (2021). **"A New Emitter Localization Technique Using Airborne Direction Finder Sensor".** *Majlesi Journal of Mechatronic Systems*, 10(4), 5-16.

[25] O. Sharifi-Tehrani, **"Design, Simulation and Fabrication of Microstrip Hairpin and Interdigital BPF for 2.25 GHz Unlicensed Band,"** *Majlesi Journal of Telecommunication Devices*, vol. 6, no. 4, 2017.

[26] O. Sharifi-Tehrani and S. Talati. (2017) **"PPU Adaptive LMS Algorithm, a Hardware-Efficient Approach; a Review on",** *Majlesi Journal of Mechatronic Systems*, vol. 6, no. 1.

[27] O. Sharifi-Tehrani, "**Hardware Design of Image Channel Denoiser for FPGA Embedded Systems,**" *Przegląd Elektrotechniczny*, vol. 88, no. 3b, pp. 165-167, 2012.

[28] O. Sharifi-Tehrani, A. Sadeghi, and S. M. J. Razavi, **"Design and Simulation of IFF/ATC Antenna for Unmanned Aerial Vehicle,"** *Majlesi Journal of Mechatronic Systems*, vol. 6, no. 1, pp. 1-4, 2017.

[29] O. S. Tehrani, M. Ashourian, and P. Moallem, **"An FPGA-based implementation of fixed-point standard-LMS algorithm with low resource utilization and fast convergence,"** *International Review on Computers and Software*, vol. 5, no. 4, pp. 436-444, 2010.

[30] O. Sharifi-Tehrani, **"Novel hardware-efficient design of LMS-based adaptive FIR filter utilizing Finite State Machine and Block-RAM,"** *Przeglad Elektrotechniczny*, vol. 87, no. 7, pp. 240-244, 2011.

[31] O. Sharifi-Tehrani, M. F. Sabahi, and M. R. Danee, **"Low-Complexity Framework for GNSS Jamming and Spoofing Detection on Moving Platforms,"** IET Radar, Sonar & Navigation, vol. 14, no. 12, pp. 2027-2038, 2020.

[32] M. Ashourian and O. Sharifi-Tehrani, **"Application of semi-circle law and Wigner spiked-model in GPS jamming confronting,"** Signal, *Image and Video Processing*, pp. 1-8, 2022.

[33] O. Sharifi-Tehrani, M. F. Sabahi, and M. Danaee, **"Null broadened–deepened array antenna beamforming for GNSS jamming mitigation in moving platforms,"** *ICT Express*, vol. 8, no. 2, pp. 161-165, 2022.

[34] O. Sharifi-Tehrani, H. Lashgarian, M. Soleymanzade, and M. H. Ghasemian, **"Futurology of Electronic Warfare Systems for IR. IRAN's Fast Crafts,"** *Majlesi Journal of Telecommunication Devices*, vol. 8, no. 2, 2019.

[35] O. Sharifi-Tehrani, A. Sadeghi, and S. M. J. Razavi, **"Design and Simulation of IFF/ATC Antenna for Unmanned Aerial Vehicle,"** *Majlesi Journal of Mechatronic Systems*, vol. 6, no. 1, pp. 1-4, 2017.

[36] O. Sharifi-Tehrani, M. F. Sabahi, and M. R. Danee, **"GNSS Jmming Detection of UAV Ground Control Station Using Random Matrix Theory,"** *ICT Express*, vol. In Press, 2020.
[37] O. Sharifi-Tehrani, **"Novel hardware-efficient design of LMS-based adaptive FIR filter utilizing Finite State Machine and Block-RAM,"** *Przeglad Elektrotechniczny*, vol. 87, no. 7, pp. 240-244, 2011.
[38] H. Pourghassem, O. Sharifi-Tehrani, and M. Nejati, **"A novel weapon detection algorithm in X-ray dual-energy images based on connected component analysis and shape features,"** *Australian Journal of Basic and Applied Sciences*, vol. 5, pp. 300-307, 2011.
[39] O. S. Tehrani, M. Ashourian, and P. Moallem, **"Fpga implementation of a channel noise canceller for image transmission,"** *in Machine Vision and Image Processing (MVIP)*, 2010 6th Iranian, 2010, pp. 1-6: IEEE.
[40] Ghazali, S. M., Baleghi, Y**. "Pedestrian Detection in Infrared Outdoor Images Based on Atmospheric Situation Estimation"** *Journal of AI and Data Mining*, 2019; 7(1): 1-16. doi: 10.22044/jadm.2018.5742.1696
[41] Talati, S., Ghazali, S. M., Hassani Ahangar, M., & Alavi, S. M. (2021). **"Analysis and Evaluation of Increasing the Throughput of Processors by Eliminating the Lobe's Disorder"** *Majlesi Journal of Telecommunication Devices*, 10(3), 119-123. https://doi.org/10.52547/mjtd.10.3.119
[42] Seyed Morteza Ghazali, Jalil Mazloum, Yasser Baleghi. **"Modified binary salp swarm algorithm in EEG signal classification for epilepsy seizure detection"** *Biomedical Signal Processing and Control*. Volume 78, September 2022, 103858.
[43] EtezadiFar. P., Talati. S., Hassani Ahangar. M.R., Molazade. M., **"Investigation of Steganography Methods in Audio Standard Coders: LPC, CELP, MELP"** *Majlesi Journal of Telecommunication Devices*, 12(1), in press, 2023.

Existence of Excitatory and Inhibitory Oscillators in The Small World Network and Its Dynamic Effect on Network Synchronization

Tayebeh Nikfard[1], Ravindra Kumar[2]
1- Department of Physics, Mobarakeh Branch, Islamic Azad University, Mobarakeh, Iran.
Email: nikfardtayebeh@gmail.com (Corresponding author)
2-Department of Physics, Radha govind University, Ramgarh 829122, India.
Email: Ravindk@gmail.com

ABSTRACT:
Synchronization was investigated in Watts-Strogats small world network with inhibited and excitable oscillators. According to the Kuramoto model in the small world network, with the increase in the limited number of inhibited oscillators, the synchronization in the system will be accompanied by network defects, and with their increase, the synchronization will also increase, and after reaching its maximum value, it will begin to decrease. That is, with a certain ratio of inhibitory oscillators to excitation depending on the coupling strength, network synchronization is maximum. As the coupling strength of the oscillators increases, the interval of the number of inhibitions for which the network is in synchronization decreases. This result is not related to a specific small world network and has been observed by repeating it in different small world networks. Excitatory and inhibitory oscillators are in phase up to a certain percentage of inhibitory oscillators in the network (depending on the coupling strength).

KEYWORDS: Kuramoto, Synchronization, Small world network, Inhibitory oscillator, Excitatory oscillator

1. INTRODUCTION

Since 1950, network science has become a living and interdisciplinary field. Today, networks play an important role for research in various fields, including social sciences, economics and psychology, biology, physics and mathematics [1,2] and as a forward-looking concept, it is used to describe the interactions of many systems. Several network models have been developed that have statistical properties consistent with real-world networks. In particular, we can mention random networks or René camp, small world network in network science.

Real-world networks such as brain networks, electrical networks, etc. [3] are characterized by a high clustering coefficient. Also, despite the large size, there is often a relatively short path between both nodes. Strugats presented a model with small-world network [3] that exhibits both features, small shortest path length and high clustering factor. These features are known as the small world feature, which consists of a regular network and is rewired with the probability p of edges, which is from 0.005 to 0.05 and is between the regular network (p = 0) and the random network (p = 1).

One of the main topics of network dynamics is synchronization [4,5]. Synchronization can be seen in many different contexts. In computer science, such as synchronization has been used to extract data in a large database [6]. Other applications in engineering where synchronization or asynchrony are important, such as wireless communication networks [7] and electric networks [8].

By simulating his model, Winfrey [9] found that spontaneous synchronization appears as a threshold process, a phenomenon similar to phase transition, and in his studies and Kuramoto [10], it is stated that the start of synchronization in Oscillating populations represent phase transitions; Below the transition point, the individual movement of oscillators in a group is uncorrelated. As their interactions become stronger, the connections between the dynamic modes of the

Paper type: Research paper
Received: 22 November 2023; revised: 17 December 2023; accepted: 28 January 2023; published: 1 March 2024
How to cite this paper: T. Nikfard, R. Kumar, **"Existence of Excitatory and Inhibitory Oscillators in The Small World Network and Its Dynamic Effect on Network Synchronization"**, *Majlesi Journal of Telecommunication Devices*, Vol. 13, No. 1, pp. 37-40, 2024.

oscillators in one part of the set are established and the frequencies of these oscillators become the same. Near the transition point, the size of the coherent oscillator group is small, but the group grows and the number of interacting oscillators increases.

The size of this group can be chosen as a synchronization parameter. Based on Winfrey's method, The Kuramoto model consists of a population of phase oscillators whose interaction is determined by differential equations [11,12] and expresses the rotation of oscillators with heterogeneous natural frequency that are coupled in the form of phase difference sinusoids.

The paper is organized as follows. In Sect. II, we define the model and the numerical methods of quantifying the synchronization. Sect. III represents the results and discussion and sect. IV is devoted to the concluding remarks.

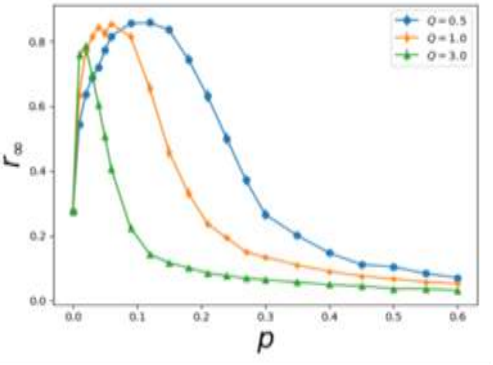

Fig. 1. (Color online) Stationary order parameters verses fraction of inhibitory oscillators for the excitatory-inhibitory model for Q = 0.5, Q = 1 and Q = 1.5 for small world (with the probability of rewiring 0.03) networks of N = 1000 oscillators and mean degree ⟨k⟩ = 10. The error bars indicate the standard error of mean (SEM).

2. MODEL AND METHOD

We used the Kuramoto model in a network with N oscillators at the nodes of the network, which include two groups. One group (excitatory oscillators) has positive coupling and tries to be in phase with its neighbor, and another group (inhibitory oscillators) tries to be in the opposite phase (π) with it.

Therefore, in the Kuramoto equations:

$$d\theta_i^s/dt = \omega_0 + (1/k_i)\sum_{j=1}^{N} a_{ij}\lambda_j^s \sin(\theta_j - \theta_i^s), \quad i = 1, \dots, N \tag{1}$$

In this equation, θ_i is the phase of the ith oscillator, ω_0 is the intrinsic frequency of the oscillators, which are equal and zero without losing any generality. a_{ij} are the elements of the adjacency matrix, where $a_{ij} = 1$, if oscillator i and j are connected, otherwise $a_{ij} = 0$, and k_i is the degree of node ith. λ_i^s is the coupling constant of the ith oscillator (s indicates excitatory and inhibitory) which λ_j^{excit} is positive if the oscillator is excitatory and λ_j^{inhib} is negative if the oscillator is inhibitory. Assuming $Q > 0$ and λ_j^{excit}, we will have: $\lambda_i^{inhib} = -Q\lambda_i^{excit}$, also $\tau = \lambda_i^f t$.

We determine the degree of synchronization of all oscillators in each time interval by the order parameter:

$$r(\tau) = \frac{1}{N}\sum_{j=1}^{N} exp(i\theta_j(\tau)) \tag{2}$$

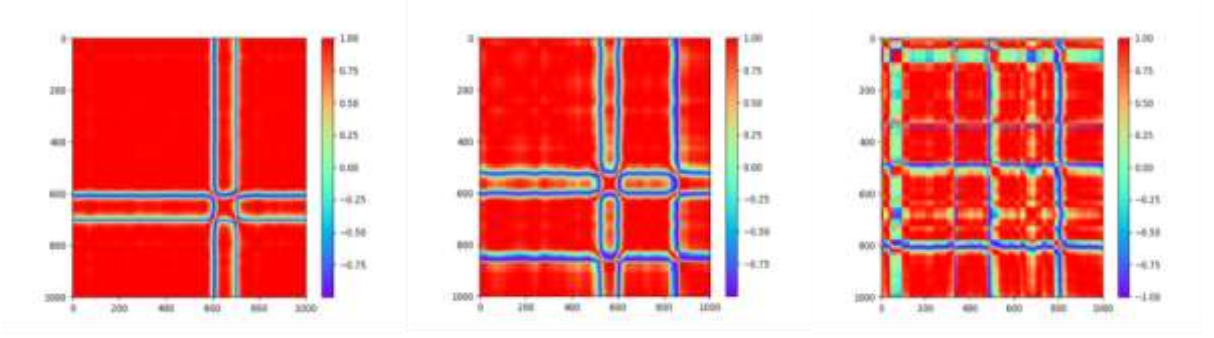

(a) (b) (c)

Fig. 2. (Color online) correlation matrix of inhibitory and excitatory oscillators for (a) p=0.03, (b)p=0.09 and (c)p=0.18 in a small world networks of N=1000 oscillators, mean degree ⟨k⟩=10 and Q=0.5. p is the fraction of inhibitory to excitatory oscillators.

We define the longtime averaged order parameter in the stationary state as:

$$r_{\infty} = \lim_{\Delta\tau\to\infty} \frac{1}{\Delta\tau} \int_{\tau_s}^{\tau_s+\Delta\tau} r(\tau) d\tau \qquad (3)$$

in which τ_s is the time of reaching a stationary state.

3. RESULTS AND DISCUSSION

We considered the model for a small world network with 1000 nodes and an average degree of 10. Note that all edges are bidirectionally selected and we denote the ratio of inhibitory oscillators to excitatory oscillators by p. To obtain the time evolution of the oscillators, we used the fourth-order Rangkota method with a time step of 0.1 and considered the initial phase of the oscillators from the box diagram in the interval [π, -π], and the natural frequency distribution of the oscillators follows the Lorentz distribution function.

We obtained the average order parameter for 150 runs for the small world network and different initial conditions and 30 runs for 10 different networks and different initial conditions. $\backsim 8\times10^5$time step calculations have been done and from this number, 1000 final steps have been kept and averaged. In the calculations, it can be seen that the time step of the network is about $\backsim 6\text{x}10^5$ and reaches a stable state.

As it is thought, the power of coupling of inhibition and excitation oscillators can be effective in the order parameter and thus network synchronization by increasing the number of inhibition oscillators in the network up to a certain percentage. In Fig. (1), three states are considered for Q: $Q < 1$, $Q = 1$, $Q > 1$. By setting γ=0 in the model, the order parameter is drawn in terms of p. For all three modes, the initial phase of the oscillators is the same. With the increase of inhibitory nodes in the network, the order parameter increases and then decreases, and the higher the coupling strength of the nodes, the faster this decrease and the resistance of the network for synchronization is lower. This turning point depends on the value of Q and decreases with increasing Q.

It can also be seen in Fig. 1 when there is no inhibitory oscillator in the network, the network has not reached full synchronization and what is shown in this figure is the average of 10 initial conditions. By increasing the inhibited oscillators in the small world network in a certain range, not only the order parameter does not decrease, but the order parameter increases up to a certain percentage of the inhibited oscillators.

For a better review, the correlation matrix for $Q = 0.5$ is drawn in Fig. 2. In this figure, it can be seen that network defects are seen for percentages of the inhibited oscillator which is the maximum order parameter. At first, when the percentage of inhibited oscillators in the network increases from zero, the network defects decrease and in fact the network becomes more regular. Then, with the increase of inhibitory oscillators, network defects increased and for higher percentages (for network with $Q = 0.5$, for $p > 0.18$, for network with $Q = 1$, for $p > 0.1$ and for network with $Q = 3$, for $p > 0.03$) disappears. In fact, around the maximum order parameter, the oscillators are divided into two groups that are in opposite phase (π).

With the investigation, we came to the conclusion that the group of oscillators that are in opposite phase with other oscillators and cause network defects, are not only inhibited oscillators and include both inhibited and excited oscillators. The presence of a small percentage of the inhibited oscillator causes a number of oscillators to be in opposite phase with the rest of the oscillators and even for a certain percentage, they create a higher order in the network.

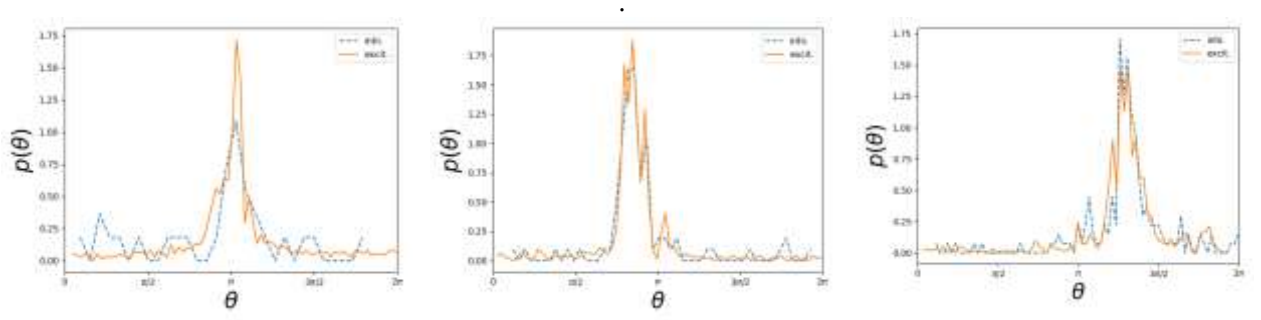

(a) (b) (c)

Fig. 3. (Color online) The probability density function of the phase of inhibitory and excitatory oscillators for (a) p 0.03,(b)p=0.09 and (c)p=0.18 in a small world networks of N=1000 oscillators, mean degree ⟨k⟩=10 and Q=0.5. p is the fraction of inhibitory to excitatory oscillators.

The phase density of the oscillators after the network reached a stable state, separately (inhibitory and excitatory) is drawn in Fig. 3 for Q=0.5 in the small world network for the percentages presented respectively in Fig. 2. As can be seen in these figures for the percentage of inhibition oscillators that we observed network defects, the phase density diagrams of inhibition and excitation oscillators are in phase.

4. CONCLUSION

In summary, using the Kuramato model in the small world network and defining inhibitory and excitatory oscillators, we found that the excitatory and inhibitory oscillators are always in phase. We also observed an increase in synchrony by increasing the fraction of inhibitors in the SW network, where the number of inhibitory oscillators to maximize synchrony depends on the coupling strength of the oscillators.

REFERENCES

[1] Solé, Ricard V, Corominas-Murtra, Bernat, Valverde, Sergi, and Steels, Luc. **"Language networks: Their structure, function, and evolution. *Complexity*,"** 15(6):20–26, 2010.

[2] Newman, MEJ. **"The structure and function of complex networks,"** siam re-view, 45, 167–256. *Cerca con Google*, 2003.

[3] Watts, Duncan J and Strogatz, Steven H. **"Collective dynamics of 'small-world'networks,"** *nature*, 393(6684):440, 1998.Plasma Sci. [Online]. 21(3), pp. 876-880. Available:

[4] Strogatz, Steven H and Stewart, Ian. **"Coupled oscillators and biological synchronization,"** Scientific American, 269(6):102–109, 1993.

[5] Keane, Andrew, Dahms, Thomas, Lehnert, Judith, Suryanarayana, Sachin Aralasurali, Hövel, Philipp, and Schöll, Eckehard. **"Synchronisation in networks of delay-coupled type-i excitable systems,"** The European Physical Journal B, 85(12):407, 2012.

[6] Miyano, Takaya and Tsutsui, Takako. **"Data synchronization in a network of coupled phase oscillators,"** Physical review letters, 98(2):024102, 2007.

[7] Díaz-Guilera, Albert, Gómez-Gardenes, Jesús, Moreno, Yamir, and Nekovee, Maziar. **"Synchronization in random geometric graphs,"** International Journal of Bifurcation and Chaos, 19(02):687–693, 2009.

[8] Rohden, Martin, Sorge, Andreas, Timme, Marc, and Witthaut, Dirk. **"Self-organized synchronization in decentralized power grids,"** Physical review letters, 109(6):064101, 2012.

[9] Winfree, Arthur T. **"Biological rhythms and the behavior of populations of coupled oscillators,"** Journal of theoretical biology, 16(1):15–42, 1967.

[10] Kuramoto, Yoshiki. **"Chemical oscillations, waves, and turbulence,"** Courier Corporation, 2003.

[11] Kuramoto, Yoshiki. **"Self-entrainment of a population of coupled non-linear oscillators,"** in International symposium on mathematical problems in theoretical physics, pp. 420–422. Springer, 1975.

[12] Y. kuramoto: **"Chemical oscillations, waves, and turbulence, springer-verlag,"** berlin and new York, 1984, viii+ 156, 25× 17cm, 9,480 ff (springer series in synergetics, vol. 19). 40(10):817–818, 1985.

An Improved Method to Evaluate the Vehicle's Encounter with Events in the VANET with the Approach of Developing Non-Linear Methods

Farzaneh Kaviani[1], Mohammadreza Soltanaghaei[2]
Department of Computer Eng., Isfahan (Khorasgan) Branch, Islamic Azad University, Isfahan, Iran.
Email: f.kavyani96@gmail.com
Department of Computer Eng., Isfahan (Khorasgan) Branch, Islamic Azad University, Isfahan, Iran.
Email: soltan@khuisf.ac.ir

ABSTRACT:
Data exchange between vehicles as network nodes, like other ad-hoc networks, due to the lack of stability infrastructure and central management, and the complete distribution of the network platform, have led to attract many parts of today's researches. In this article, an improved method has been presented in order to evaluate the encounter of the vehicle with the incident, and the interaction of data related to the incidents for use in the vehicle ad-hoc networks. The proposed method has been developed based on the basic indicators of evaluating the node's encounter with events in vehicle ad-hoc networks and has been strengthened based on the advantages and capabilities of fuzzy logic, so that the desired and expected result is obtained from the output of the set. In order to evaluate the performance of the proposed method, developments and implements were based on the OPNET simulator and this method was compared with the VESPA and VESPA-DM methods as the most important researches in this field. The simulation results indicated the superiority of the proposed method over past researches.

KEYWORDS: Vehicle Ad Hoc Networks, Evaluation of Vehicle Encounters with Events, Event Sharing Management, Fuzzy Logic.

1. INTRODUCTION

In today's world, vehicles are considered as the most used means of transportation. Unfortunately, the popularity of this widely used tool has come with several issues such as security and environmental issues. Therefore, in order to reduce vehicle accidents, several programs, which are generally related to the intelligent system of vehicles, have been started in Japan, America and some European countries and they have attracted the attention of many scientific and industrial researchers. The result of this research was the introduction of ADAS (advanced driver assistance system) [1 and 2]. Furthermore, wireless networks were expanded and made it possible to establish wireless IVC (Inter-Vehicle Communications) communication between vehicles. The main purpose of these communications was to increase the security of the vehicle network and its management by exchanging information between nearby vehicles [2]. For example, IVC provides the ability to notify vehicle occupants (through nearby vehicle) of an accident that has occurred on the road ahead of them, or to notify them of an incident in the area. Thus, there is a fundamental difference between Advanced Driver Assistance System (ADAS) and IVC. ADAS provides the ability to analyze data based on information stored on an external memory, while IVC supports and implements IVC during movement [3 and 4].

IVC inter-vehicle wireless communication based on standards such as IEEE802.11p or UWB provides the ability to support wireless network communication with a short range (several hundred meters), and a bandwidth of about megabits/second. [5] Based on the use of such wireless communication technology, network nodes are able to share information related to accidents, parking space, traffic level, etc. [4, 6]. While there are networks with a wide range and

Paper type: Research paper
Received: 22 November 2023; revised: 17 December 2023; accepted: 28 January 2024; published: 1 March 2024
How to cite this paper: F. Kaviani, M. Soltanaghaei, **"An Improved Method to Evaluate the Vehicle's Encounter with Events in the VANET with the Approach of Developing Non-Linear Methods"**, *Majlesi Journal of Telecommunication Devices*, Vol. 13, No. 1, pp. 41-48, 2024.

high throughput such as GPRS, UMTS (mobile phone networks), but these types of networks do not support the dynamic characteristics of nodes in the network [7]. On this basis and for the quick exchange of information between two vehicles, they will not be effective and practical in order to prevent an accident. Often, these types of technologies can be used in applications such as finding different places, etc.

In vehicle ad hoc networks, in very high mobility and the non-uniform and random movement of nodes [8 and 9], information management is considered a very important and big challenge that the some of these challenges related to this topic will be addressed below:

• Is it necessary to report the information to the driver or send a warning to the driver depending on the location of the vehicle in relation to the information exchanged (shared event).

• What necessary information is reported and what information needs to be provided to other vehicles;

• How should the sharing of information related to events be done (what time and place) so that, in addition to being effective, it does not negatively affect network resources.

In relation to these concepts and challenges, the place and time dimension (the vehicle in relation to the published event) is very important, and correct and optimal decision-making in this connection can play a useful and effective role in improving performance. The high importance of this topic in vehicle networks shows the necessity of providing effective research to improve this field.

In this article, an improved method has been introduced based on the basic indicators of evaluating the vehicle's encounter with the event, focusing on the performance of fuzzy sets. The proposed method consists of two stages of evaluating the encounter of the vehicle with the event and re-sharing the event message. Based on these two stages, it is tried to evaluate the encounter and manage the sharing of events in a favorable way in the context of vehicle networks. The proposed method, based on the operational framework of its stages, provides the ability to evaluate the node's encounter with the event with high accuracy and tries to share the received events with other nodes in the network.

The parts of the article are: the second part is related work, the third part is the approach of the article, the fourth part is the introduction of the proposed improved method, the fifth part is the simulation, the experimental results and the efficiency analysis of the proposed method, and finally, in the sixth part, the summary of the article is presented..

2. RELATED WORK

According to what was presented and considering the importance of the subject of evaluating the vehicle confrontation with the event and its sharing in the vehicle networks, so far, several researches have been presented in this basic field. In this part of the article, we will review some of the most important ones. The purpose of this review is to show the importance of the present article in order to improve the open challenges in the field of evaluating the vehicle encounter with the event and its sharing. Most of the presented articles suffered from neglecting the important and basic indicators of evaluating the vehicle confrontation with the event.

In [10 and 11], crash warning assistant systems have been proposed with the aim of improving the problem of outside the line of sight. In this research, an attempt has been made to evaluate the two factors of the time of encountering an accident and the time of preventing an accident. In [12], methods for message propagation with the aim of minimizing packet delivery delay, which is considered essential in the safety applications of vehicle ad hoc networks, have been proposed. The introduced method works in accordance with congestion control policies and based on the release of safety-emergency packets [13]. In [14 and 15], techniques based on multi-hop propagation of packets with the aim of preventing chain accidents have been proposed. In [16], the traffic visibility of vehicles on multi-lane roads has been investigated. In this work, three types of protocols contain propagation by nodes in the same direction, propagation by nodes moving in the opposite direction, and propagation by nodes moving in both agreeing and opposing directions, are used to analyze the rate of receiving data and the average error rate and [17]. In [18], opportunistic methods derived from medical science are proposed, in such a way that information acts like a disease vector and is transmitted to nearby nodes. In [19-21], other opportunistic methods have been proposed. In these methods, time indicators, and the optimal space are taken into consideration. In the following, three classic storm strategies, epidemic strategy, and proximity are examined. In [22], a method for scaled broadcast based on node position, time condition and information condition is proposed. In [23-25], the probability of an accident and encounter of node with the desired accident have been investigated, and a solution has been suggested for how to pass the accident. In this work, fuzzy logic has been used to evaluate the encounter with an accident. In [26], based on the segmentation of the network platform (city), publications are made in an intelligent manner, based on the importance of the message. In method of [27], the network is divided into separate areas, and based on this, network releases are made so that an implicit control is applied on the release. In [4] and [28], methods aimed at classifying events, evaluating the probability of a node encountering an event, and managing its re-release are proposed. These evaluations have been strengthened in [28], focusing on the advantages of using digital maps in order to increase the accuracy of calculations. In [29-30], the issue of places with low density of vehicles and disruptions in sending messages has been discussed.

In [31] addresses these challenges by proposing a decentralized Blockchain based trust management framework (BC-TMF) aiming to compute trust metrics for vehicles. These trust metrics rely on the authenticity of the messages. Periodically each miner aggregates the received trust metrics into global trust metrics, then packs them in a block.

In [32] proposed an Artificial Intelligence (AI)-based Sugeno fuzzy inference system. The proposed Artificial Intelligence (AI)-based Sugeno fuzzy inference system provides network security, reduces end-to-end delay, and increases packet delivery ratio and throughput. S Nagpal el al. 2022 [33] is focusing on assorted assaults on the VANET environment so that a detailed view of vulnerabilities can be analysed. In addition, the assorted security mechanisms and approaches are underlined and explained to guard against the assaults effectively with a higher degree of performance. In year of 2023 [34] quantifies VANETs to improve their reliability and availability, essential for integrating urban advanced mobility (UAM) into urban infrastructures This research is significant for monitoring UAM systems in future cities, presenting a cost-effective framework over traditional methods and advancing VANET reliability and availability in urban mobility contexts. In [35] proposed a security system based on intrusion detection called Detection of Anomalous Behaviour in Smart Conveyance Operations (DAMASCO). They used a statistical approach to detect anomalies in vehicle-to-vehicle communication (V2V). In [36] discussed the detection and a deep analysis of affects of malicious nodes on the network performance as throughput, average latency, and packets drop in the network. They presented an approach to detect malicious data with Artificial Neural Networks as well as malicious nodes with Support Vector Machines in VANETs. In E Al-Ezaly et al. 2023 [37] used vehicular ad-hoc networks (VANETs) for VANET traffic light recognition (VTLR). Information exchange as well as monitoring of the TL status, time remaining before a change, and recommended speeds are supported.

The past researches suffered the lack of evaluating the variety of events, and some limitations such as increasing the error coefficient of linear equations, and the accuracy of calculations. In this article, the focus has been on providing a method based on important indicators in evaluating the node's encounter with the event and its re-release. These indicators are developed based on the performance of multi-level fuzzy logic to improve the disadvantages and problems of linear and threshold-based decision making. Also, an attempt has been made to use other new indicators in order to improve the accuracy of decision-making and the performance of the proposed method based on wider indicator.

3. PROPOSED METHODS

The proposed fuzzy set is a multi-level set and it is based on Mamdani's fuzzy logic, which is based on a series of if and then rules to derive outputs based on inputs (Fig. 1).

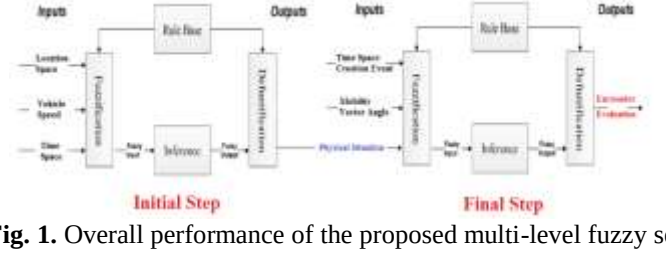

Fig. 1. Overall performance of the proposed multi-level fuzzy set

Finally, based on the function of fuzzy logic, the final result of evaluating the node's encounter with the event is deduced. The final output membership functions are shown in Fig. 2. The higher the output value or encounter probability tends to one (VHigh), the higher the encounter probability.

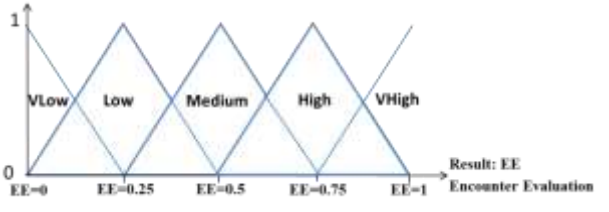

Fig. 2. The final output functions of the proposed fuzzy set.

In relation to the results obtained from the proposed two-stage fuzzy set, if the fuzzy output is obtained in VLow mode, it means that the vehicle will not encounter an event in terms of all the valuable criteria. Therefore, the event

message is worthless in this situation, and the desired node ignores its re-broadcast in order to prevent unnecessary traffic injection into the network and to prevent the negative effects of unnecessary message dissemination. The flowchart of the proposed method along with its operational components is shown in Fig. 3.

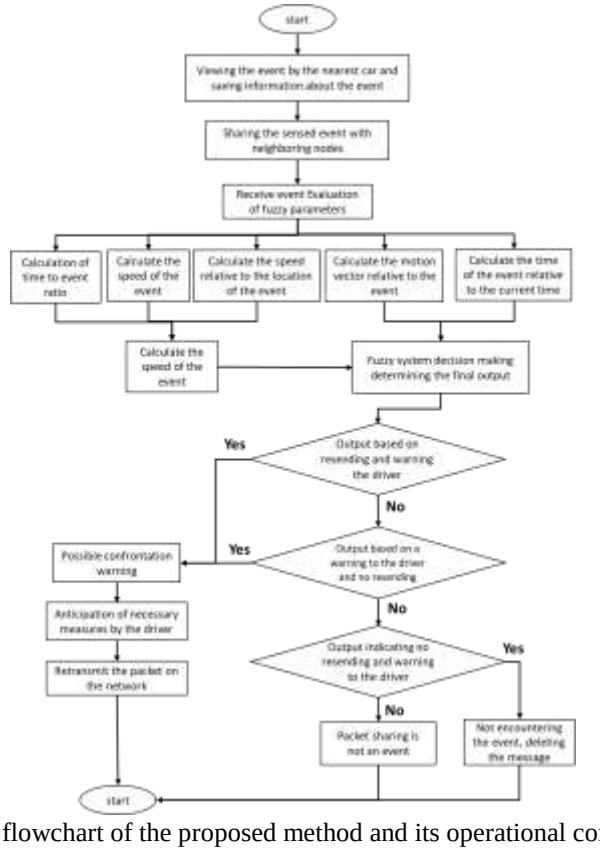

Fig. 3. The flowchart of the proposed method and its operational components.

4. SIMULATION AND EXPERIMENTAL RESULTS

In order to show the effectiveness of the proposed method in the area covered by the article, it has been simulated with the OPNET simulator software. A vehicle ad-hoc network has been designed and simulated using physical layer protocols and MAC (media access control) in IEEE802.11p in the OPNET simulator, and the methods under comparison have been developed based on it. The parameters related to the simulation scenarios are according to the parameters presented in table (1). The proposed method has been compared to VESPA [4] and VESPA-DM [15] for the purpose of comparisons and evaluation.

Table 1. Parameters related t

Parameter	Value
Simulation time	900 s
Start of simulation time	100 s
Vehicle number	100, 150, 200
Network area	10000 m * 10000 m
Vehicle mobility model	Random way point in identified route
The type of traffic sent after the event	Constant Bit Rate (CBR)/UDP
The volume of event packets	1024 byte
Operating mode	802.11p
Transfer rate	27 Mb/s, 6 Mb/s
The speed of node mobility	Randomly between 0-33 m/s (120 km/h)
Create an event	In constant period of time

Fig. 4 shows the rate of receiving published events and Fig. 5 shows the network loading rate in different scenarios. The reception rate is the average number of received event messages and the network loading rate, including the total amount of traffic sent in the network platform for the publication of events. It is reasonable to improve the network resources, including overhead, unnecessary traffic injection, increased calculations and loading, etc. If the compared methods, including the VESPA and VESPA-DM methods have an increase in the error coefficient (error coefficient Astana) and the lack of purposeful decision-making in the accompanying publications, due to the neglect of some important criteria for confrontation evaluation, the use of linear calculations and threshold-based decision-making, which has led to an increase in unnecessary sharing and an increase in network workload and unnecessary traffic injection into the network.

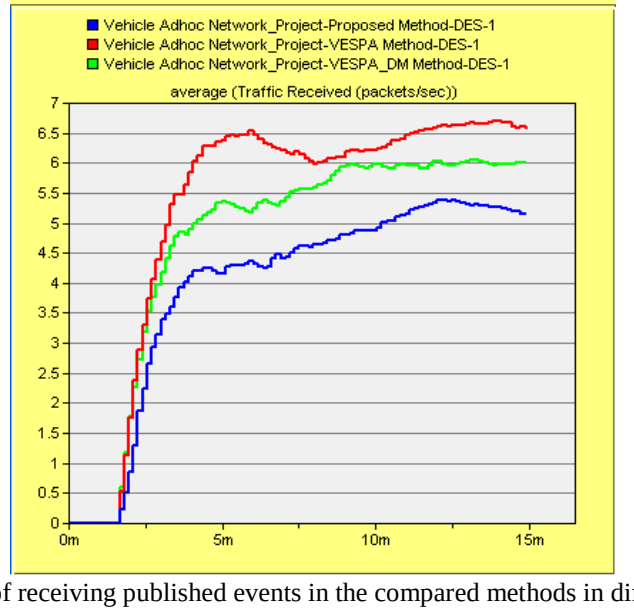

Fig. 4. The rate of receiving published events in the compared methods in different scenarios

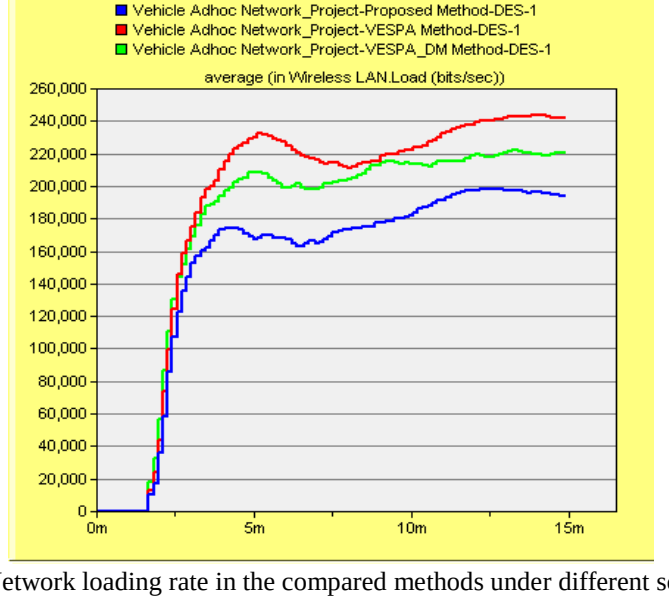

Fig. 5. Network loading rate in the compared methods under different scenarios

Fig. 6 shows the propagation delay and Fig. 7 shows the network efficiency in different scenarios. Event propagation delay is the average delay required to propagate events in the vehicles of the relevant area. The network efficiency includes the evaluation of the correct encounter of the node with the event and the management of the occurrences and will change related to the amount of network load and the propagation delay. These criteria will be improved according to how the methods work in the amount of calculations and the speed of calculations. If the number of releases and

updates are optimized and done with higher management, the delay of releases will decrease and the efficiency rate will increase. The performance of the proposed method based on the use of multi-level fuzzy logic and the stated application criteria has increased the speed of decision-making, and has led to the improve and manage the publication of messages related to events at the vehicle network level and optimize sharing of information with the vehicles, which has ultimately reduced the delay and increased the efficiency of the network. In the both VESPA and VESPA-DM methods, due to neglecting some important criteria for confrontation evaluation, and due to the use of applied linear equations in their research, with the lack of optimal sharing and the increase of the error coefficient related to Linear calculations have been associated, which have been associated with increasing delay and decreasing efficiency. On the other hand, the VESPA-DM method, based on the increase in accuracy in performance, based on a digital map, has been more efficient than the VESPA method, especially in relation to moving events, and has been associated with improvement.

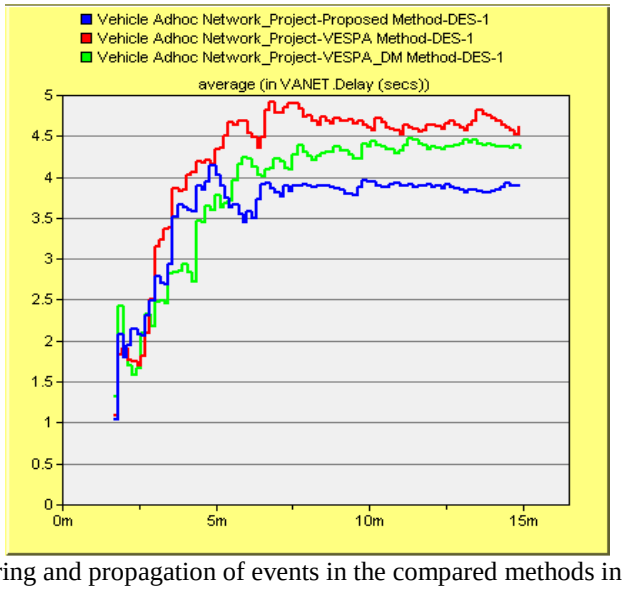

Fig. 6. Delay of sharing and propagation of events in the compared methods in different scenarios.

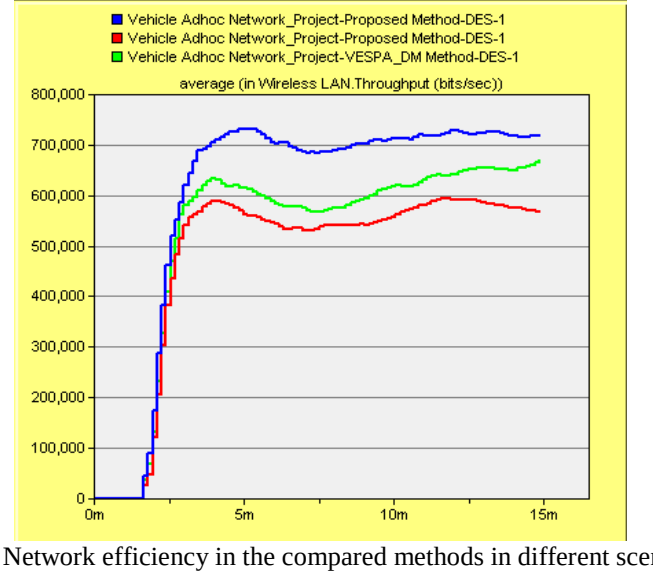

Fig. 7. Network efficiency in the compared methods in different scenarios

5. CONCLUSION AND FUTURE WORK

In this article, a mechanism for assessing the node's encounter with the event and its re-release was introduced with the aim of increasing the accuracy in the calculations of encounter with the published event, and optimizing the exchanges of vehicular networks. The performance of the proposed method has improved the criteria related to the evaluation of the encounter and the exchange management of car networks compared to the previous methods. In the

future works, we are trying to make the proposed method more optimal and practical by using predictive criteria such as Markov chain and other criteria related to the evaluation of the vehicle's encounter with the event in the vehicle networks.

REFERENCES

[1] Vadivel, Sharmila, et al. "**Dynamic route discovery using modified grasshopper optimization algorithm in wireless Ad-Hoc visible light communication network**." Electronics 10.10 (2021): 1176.

[2] S Lin, Chia-Hung, et al. "**A survey on deep learning-based vehicular communication applications**." Journal of Signal Processing Systems 93.4 (2021): 369-388.

[3] Wang, Xiaoyan, et al. "**Better platooning toward autonomous driving: Inter-vehicle communications with directional antenna**." China Communications 18.7 (2021): 44-57.

[4] T. Delot, N. Cenerario, and S. Ilarri, "**Vehicular event sharing with a mobile peer-to-peer architecture**," Transportation Research Part C, Vol. 18, pp. 584–598, 2010.

[5] Singh, Pranav Kumar, Sunit Kumar Nandi, and Sukumar Nandi. "**A tutorial survey on vehicular communication state of the art, and future research directions**." Vehicular Communications 18 (2019): 100164.

[6] Yeferny, Taoufik, and Sofian Hamad. "**Vehicular ad-hoc networks: architecture, applications and challenges.**" arXiv preprint arXiv:2101.04539 (2021).

[7] Sharef, Baraa, et al. "**Robust and trust dynamic mobile gateway selection in heterogeneous VANET-UMTS network.**" Vehicular communications 12 (2018): 75-87.

[8] Tian, Jin, and Fudong Meng. "**Comparison Survey of Mobility Models in Vehicular Ad-Hoc Network (VANET)**." 2020 IEEE 3rd International Conference on Automation, Electronics and Electrical Engineering (AUTEEE). IEEE, 2020.

[9] Andrade, Everaldo, et al. "**Analyzing cooperative monitoring and dissemination of critical mobile events by VANETs.**" Wireless Networks 27.3 (2021): 1981-1997.

[10] Madhuri, K., and B. UmaMaheswari. "**Adaptive Steering Control and Driver Alert System for Smart Vehicles**." 2019 3rd International Conference on Computing Methodologies and Communication (ICCMC). IEEE, 2019.

[11] Miller, and Ronald, "**An adaptive peer-to-peer collision warning system,**" In: Vehicular Technology Conference, pp. 317-321, 2002.

[12] X. Yang, J. Liu, F. Zhao, and N. Vaidya, "**A Vehicle-to-Vehicle Communication Protocol for Cooperative Collision Warning**," Mobile and Ubiquitous Systems: Networking and Services, (MOBIQUITOUS), the First Annual International Conference, Vol. 11, pp. 35-43, 2004.

[13] Chehri, Abdellah, et al. "**Realistic 5.9 GHz DSRC vehicle-to-vehicle wireless communication protocols for cooperative collision warning in underground mining**." Smart Transportation Systems 2020. Springer, Singapore, 2020. 133-141.

[14] X. Shouzhi, H. Zhou, C. Li, and Y. Zhao, **"A Multi-Hop V2V Broadcast Protocol for Chain Collision Avoidance on Highways,**" Communications Technology and Applications, (ICCTA'09), Vol. 13, pp. 126-135, 2009.

[15] Urmonov, Odilbek, and HyungWon Kim. "**A multi-hop data dissemination algorithm for vehicular communication**." Computers 9.2 (2020): 25.

[16] T. Nadeem, P. Shankar, and L. Iftode, "**A comparative study of data dissemination models for VANETs,**" In: Third International Conference on Mobile and Ubiquitous Systems (MobiQuitous), pp. 1–10, 2006.

[17] Shahwani, Hamayoun, et al. "**A comprehensive survey on data dissemination in Vehicular Ad Hoc Networks**." Vehicular Communications (2021): 100420.

[18] B. Xu, A.M. Ouksel, and O.Wolfson, "**Opportunistic resource exchange in inter-vehicle ad-hoc networks**," In: Fifth International Conference on Mobile Data Management (MDM), pp. 4–12, 2004.

[19] Azimi Kashani, A., M. Ghanbari, and A. M. Rahmani. "**Improving performance of opportunistic routing protocol using fuzzy logic for vehicular ad-hoc networks in highways**." Journal of AI and Data Minining (2020).

[20] S. Nittel, M. Duckham, and L. Kulik, "**Information dissemination in mobile ad-hoc geosensor networks,**" In: Third International Conference on Geographic Information Science (GIScience), Vol. 3234, pp. 206–222, 2004.

[21] Tomar, Ravi, Hanumat G. Sastry, and Manish Prateek. "**A novel protocol for information dissemination in vehicular networks**." International Conference on Internet of Vehicles. Springer, Cham, 2019.

[22] Fahad, Muhammad, et al. "**Grey wolf optimization based clustering algorithm for vehicular ad-hoc networks**." Computers & Electrical Engineering 70 (2018): 853-870.

[23] T. Kosch, C. J. Adler, S. Eichler, C. Schroth, and M. Strassberger, "**The scalability problem of vehicular ad hoc networks and how to solve it**," IEEE Wireless Communications, pp. 22–28, 2006.

[24] V. Milanés, J. Pérez, J. Godoy, and E. Onieva, "**A fuzzy aid rear-end collision warning / avoidance system,**" Expert Systems with Applications, Vol. 39, pp.9097-9107, 2012.

[25] Basjaruddin, Noor Cholis, Didin Saefudin, and Anggun Pancawati. "**Hardware Simulation of Rear-End Collision Avoidance System Based on Fuzzy Logic**." Jurnal Rekayasa Elektrika 16.1 (2020).

[26] Rashid, Sami Abduljabbar, et al. "**Prediction Based Efficient Multi-hop Clustering Approach with Adaptive Relay Node Selection for VANET**." J. Commun. 15.4 (2020): 332-344.

[27] J. S. Li, I. Liu, C. Kao and C. Tseng, "**Intelligent Adjustment Forwarding: A compromise between end-to-end and hop-by-hop transmissions in VANET environments**," Journal of Systems Architecture, Vol. 59, pp. 1319-1333, 2013.

[28] T. Delot, S. Ilarri, N. Cenerarioa, and T. Hien, "**Event sharing in vehicular networks using geographic vectors and maps**," Mobile Information Systems, Vol. 7, pp. 21-44, 2011.

[29] K. N. Qureshi, A. H. Abdullah, and J. Lloret, "**Road Perception Based Geographical Routing Protocol for Vehicular Ad Hoc Networks**," International Journal of Distributed Sensor Networks, Vol. 5, pp. 1-17, 2016.
[30] Qureshi, Kashif Naseer, et al. "**Improved road segment-based geographical routing protocol for vehicular ad-hoc networks**." Electronics 9.8 (2020): 1248.
[31] Gazdar T. , Alboqomi O. , et al. (2022). "**A Decentralized Blockchain-Based Trust Management Framework for Vehicular Ad Hoc Networks**", [2624-6511], 5(1):348-363.
[32] Gayathri, M and C Gomathy. "**Ai-Tasfis: An Approach to Secure Vehicle-to-Vehicle Communication**." Applied Artificial Intelligence, vol. 36, no. 1, 2022, p. 2145636.
[33] Nagpal, Shally et al. "**Privacy and Security Issues in Vehicular Ad Hoc Networks with Preventive Mechanisms**." Proceedings of International Conference on Intelligent Cyber-Physical Systems: ICPS 2021, Springer, 2022, pp. 317-329.
[34] Silva, Luis Guilherme et al. "**Urban Advanced Mobility Dependability: A Model-Based Quantification on Vehicular Ad Hoc Networks with Virtual Machine Migration**." Sensors, vol. 23, no. 23, 2023, p. 9485.
[35] Valentini, Edivaldo Pastori et al. "**A Novel Mechanism for Misbehaviour Detection in Vehicular Networks**." IEEE Access, 2023.
[36] Sharan, Bhagwati et al. "**A Novel Approach for Malicious Node Detection in Vehicular Ad-Hoc Network Using Support Vector Machine.**" 2023.
[37] Al-Ezaly, Esraa et al. "**An Innovative Traffic Light Recognition Method Using Vehicular Ad-Hoc Networks**." Scientific reports, vol. 13, no. 1, 2023, p. 4009.

Cancer Diagnosis in Endoscopic Images using Discrete Wavelet Transform

Sinan Ghanem Mikhwir[1], Mehran Emadi[2]
1- Master student in Computer Engineering, Isfahan (Khorasgan) Branch, Islamic Azad University Isfahan, Iran
Email: sinan_gh2000@yahoo.com
2- Assistant Professor, Department of Electrical Engineering, Mobarakeh Branch, Mobarakeh, Isfahan, Iran
Email: emadi.mehran49@gmail.com (Corresponding author)

ABSTRACT:
Stomach cancer destroys the tissues of the digestive system. This cancer is one of the deadliest diseases. Endoscopic imaging is used to diagnose cancer. In endoscopy, the diagnosis of gastric cancer is difficult due to the similarity of the tissues, the low contrast of the image and the background. In order to overcome these problems, discrete wavelet transform has been used to detect stomach cancer. In the proposed method, there are data registration, data preprocessing, feature extraction, dimensionality reduction, and classification. The features are extracted with the help of discrete wavelet transform and then dimension reduction is done with the help of principal component analysis. The proposed approach was evaluated on datasets collected from five classes, including gastritis, ulcer, esophagitis, bleeding, and healthy. random forest has a value above 99% in all evaluation criteria, which represents the advantages of this category. RF is ensemble classifier that can perform well in cancer detection The results of this research show that this method is accurate and reliable in diagnosis.

KEYWORDS: Diagnosis, Destroyed tissues, Endoscopic Images, Based Stomach.

1. INTRODUCTION

Perishability from esophageal cancer remains high against advances in medical treatment. Although the propagation of esophageal squamous cell carcinoma stays unchanged, the propagation of esophageal adenocarcinoma has incremented over time. Gastroesophageal reflux disease (GERD) and obesity are factors in the development of Barrett's esophagus and subsequent adenocarcinoma . Early detection of this disease can lead to the removal of esophageal cancer before lymphatic vascular invasion occurs[1-3]. Various methods have been performed for correction. Precancerous lesions and esophageal cancer Primary[4]. Chromondoscopy, narrow-band imaging, and endoscopic ultrasound examination are commonly used to evaluate primary lesions of the esophagus and stomach. Video endoscopy is a standard gastrointestinal screening method[5]. It is a less aggressive procedure used for early detection of gastric diseases. Manual search of large numbers of gastric frames is a comprehensive and time-consuming task and requires expertise. Conversely, several computer-aided detection systems have been suggested by researchers to deal with the problem of manual inspection of large volumes of frames[6-12]. Artificial intelligence (AI) is considered as a potential solution to reduce detection challenges. In recent years, artificial intelligence has made significant progress in endoscopic image diagnosis, including colorectal polyp detection, detection of Helicobacter pylori infection [13-16], and upper gastrointestinal cancer diagnosis [١۴]. In the method based on machine learning, pattern recognition processes are used. In this category of methods, after applying pre-processing on the image, numerous features including textural, spectral, geometric and statistical features are extracted from the desired image[10, 17-19]. These features are reduced in another step with the help of methods based on principal component analysis (PCA), independent component analysis (ICA). At this stage, feature selection methods can be used to select the most effective features [١۶-١٩]. Several researches have been presented in order to diagnose breast cancer. Rodriguez-Diaz and Singh [٢٠]proposed a method based on good criteria for diagnostic purposes. Veronese et al [17] suggested a computer-aided research for gastric

Paper type: Research paper
Received: 26 Ocotber 2023; revised: 15 December 2023; accepted: 25 January 2024; published: 1 March 2024
How to cite this paper: S. Gh. Mikhwir, M. Emadi, **"Cancer Diagnosis in Endoscopic Images using Discrete Wavelet Transform"**, *Majlesi Journal of Telecommunication Devices*, Vol. 13, No. 1, pp. 49-57, 2024.

cancer diagnosis based on the use of apparent features in co focal images. In [۲۱] suggested a method based on HD endoscopic images for automatic detection of esophageal lesions. In [۲۲] suggested a new method that computes local texture and color features based on Gabor-filtered original images for automatic early cancer detection in high-resolution endoscopic images. In [۲۳] illustrated a real-time and computationally efficient bleeding detection technique using wireless capsule endoscopy (WCE) technology. In [۲۴]conducted a study to test the possibility of classifying Adenocarcinoma in endoscopic images. In [۲۵]used Endoscopic ultra sonography (EUS) to diagnose esophageal cancer. In [۲۶] used computer vision techniques to correctly predict the presence of dysplastic tissue in VLE images. In [۲۴] presented deep learning on adenocarcinoma and BE disease images applied to the given dataset. In [۲۷] introduced restricted Boltzmann machines in the field of classification of the "MICCAI 2015" dataset. Using a convolutional neural network (CNN), Liu et al. proposed to automatically classify esophageal cancer (EC) and distinguish it from premalignant lesions [۲۸]Chen et al. have used deep learning to detect esophageal cancer [۲۹]. In the last decade, there are many tendencies towards feature extraction with thin representation. Because in this representation, there are almost only a small number of non-zero coefficients, or they have been thinned after applying transformations on the image. This trend seems to be due to the potential to reconstruct a signal or image from a smaller number of measurements than conventional methods to reconstruct an entire signal. The features extracted in thin transformations are more unique. One of the notable thin transforms is the use of wavelet transform. The purpose of wavelet transform is a desirable strategy to establish an optimal balance between time accuracy and frequency accuracy[36]. At higher frequencies, the wavelet transform gains temporal information at the cost of losing frequency information. While at lower frequencies, it gains frequency information at the cost of losing temporal information. This favorable approach to information exchange is useful for digital signal processing and music applications. Because events that happen at high frequencies and events that happen at high frequency usually need high frequency accuracy. Early detection of gastric cancer is important to improve patient survival, but accurate diagnosis of superficial neoplasms in the stomach is difficult even for experienced doscopists. It is believed that the computer-aided diagnostic system is an important method to provide accurate and rapid assistance to endoscopists in the diagnosis of gastric cancer. In this research, a new method based on thinning transformations using multiple classifications will be developed to detect gastric cancer using endoscopic images, and the purpose of our study will be to evaluate the system's ability. In the following, this article is divided as follows. In the second part, the wavelet transform will be introduced as a thinning transform. In the third part, the proposed method is presented. In the fourth part, the evaluation of the proposed method will be done. Finally, in section 5, the conclusion of the article will be presented.

1.1. Discrete Wavelet Transform

Wavelet transform is a desirable strategy to establish an optimal balance between time accuracy and frequency accuracy. At higher frequencies, the wavelet transform gains time-domain information at the cost of losing frequency-related information. While at lower frequencies, it gains frequency information at the cost of losing temporal information [36]. This favorable approach to information exchange is useful for digital signal processing and music applications. Also, events that occur at high frequency usually require high frequency accuracy. As the Fourier transform is defined based on an integral, the wavelet transform can also be defined based on an integral as follows(1)

$$W_{X(S,U)} = \int_{-\infty}^{+\infty} X(t)\Psi_{s,u}(t)dt \qquad (1)$$

In the above integral, the input signal x(t) is related to the wavelet by means of the transfer parameter u and the coherence parameter s. This transform transforms a signal into coefficients that represent time-frequency information. These coefficients have more time accuracy at high frequencies and more frequency accuracy at low frequencies. The homogeneity parameter enables the wavelet to exchange information in frequency events. One of the fast ways to calculate the wavelet transform is to use filters. The input signal is passed to two filters, H and G: these filters produce two sets of coefficients, both of which are sampled by a factor of two. As seen in Figure 1, this method is successively applied to a set of coefficients that come out of the H filter [37].

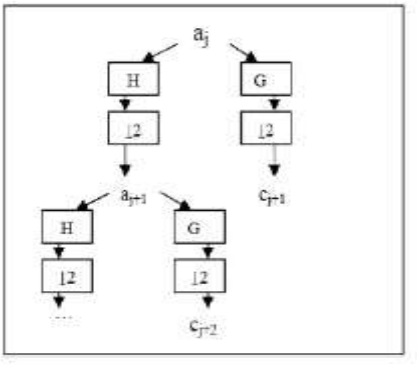

Fig. 1. Fast Wavelet Transformation using Filters[۳۰].

The DWT method overcomes the drawbacks and weaknesses of the fast Fourier transform (FFT). Signal analysis based on FFT works well when its frequency spectrum is not dependent on time, in other words, it is statistically stationary, but many signals are non-stationary in nature[38]. Time-frequency representation of time series signals is an attractive way to capture frequency information at low frequencies and time information at high frequencies. The DWT method is one of the techniques based on multi-resolution analysis [39]. For the X(t) signal, the wavelet transform is defined as follows: [۳۱].

$$WT_x(j,k) = \frac{1}{\sqrt{a_0^j}} \int x(t) \Psi^* \left(\frac{t - k a_0^j b_0}{a_0^j} \right) dt \qquad (2)$$

In equation (2), x(t) and Ψ are the initial signal and the wavelet transform function, respectively, and also the transmission parameter and a_0^j is the scale parameter. where j represents the wavelength. Usually $a_0 = 2$, so scales are sampled during a binary sequence. The sample time domain is specified using kb_0.

At each level of analysis, approximation coefficients CA and detail coefficients CD are created by passing the X(n) signal through the high-pass H and low-pass L filters [40]. Approximation coefficients and detail coefficients are obtained by the following equations:

$$CA_j = \sum_{n=-\infty}^{\infty} X_{j-1}(n) l(n - 2k) \qquad (3)$$

$$CD_j(k) = \sum_{n=-\infty}^{\infty} X(n) l(n - 2k) \qquad (4)$$

After separating the signal into high and low frequencies in the first level, only the low frequency part of the wavelet transform is taken in the next steps. By putting together the coefficient of approximation of the last level and the detail coefficients of all levels, it is reconstructed [۳۰].

2. PROPOSED METHOD

Machine learning-based methods should distinguish healthy from unhealthy tissues, including gastritis, ulcers, esophagitis, and bleeding. In machine learning, there are stages of image preprocessing, feature extraction, feature selection and finally classification. In this article, filter-based methods are used for the pre-processing of stomach images obtained from endoscopy. Then the features based on discrete wavelet transform will be extracted. It is suggested in the reduction after PCA. Finally, the selected features will be classified with the help of support vector machine, K nearest neighbor and random forest classifiers. Figure 2 depicts the proposed method. In the following, the proposed method will be explained in detail. A two-way filter is used for the pre-processing of endoscopic images. This filter is used as an edge preservation tool in image enhancement applications [42]. Along with a low-pass spatial kernel (which helps with smoothing), it uses a kernel to prevent smoothing near edges. As a result, the filter is able to smooth homogeneous areas and preserve sharp edges at the same time. In feature extraction, useful information is drawn in the space of low-dimensional features. In other words, the unique characteristics of an event such as an endoscopic image are calculated during different processes[41]. Usually, the extracted segments have smaller dimensions than the signal. Image thinning features are based on multi-resolution transformations called discrete wavelet transformation. Wavelet bases are

efficient in wavelet transformation for non-stationary endoscopic image analysis. Many researchers have used DWT to analyze endoscopic images. Basically, the Dubichse basis creates orthogonal wavelet filters. It has been used to analyze endoscopic images. Several classes of wavelet filters have been used to analyze non-stationary signals. The choice of a particular wavelet filter depends on the given application and the type of signal to be analyzed. Daubechies orthogonal wavelet filters are considered as a suitable choice for analyzing pre-processed endoscopic images in this research. This wavelet filter base has maximum smoothness or regularity. Daubechies wavelet filter banks are optimally designed for accurate signal analysis. Figure 3 shows a wavelet transform of an image at a level. As can be seen from Figure 3, with the increase in the number of wavelet conversion levels, the signal information in the high frequency (detail) and low frequency (approximation) sections decreases[44]. In this research, high frequency and low frequency information is used at level one.

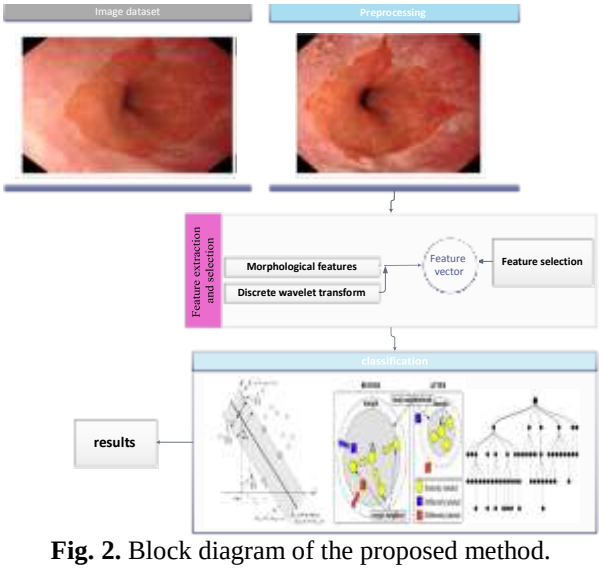

Fig. 2. Block diagram of the proposed method.

It has been used for reduction after principal opponents analysis. For a data matrix with zero empirical mean, where each row is a set of observations and each column is data corresponding to an index [45].

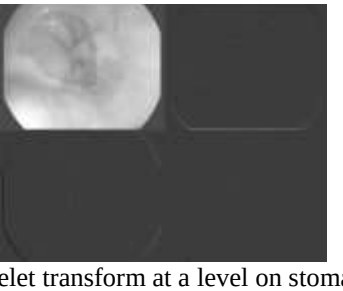

Fig. 3. Wavelet transform at a level on stomach image.

In order to reduce the dimension and remove duplicate information, principal component analysis has been used in this research. Finally, the features of the given dimension cache will be classified by three classes of support vector machine, K nearest neighbor and random forest.

3. EVALUATION

In this article, four classes of stomach disease are diagnosed along with the healthy class. In the proposed method, after pre-processing, the features of the multi-day field were extracted based on the discrete wavelet transform. Then dimension reduction was done using PCA method. In the end, classification is done with support vector machine, random forest and k nearest neighbor. In this research, the identification rate criterion was used to evaluate the proposed method. The measures used are recall rate (Equation 5), precision (Equation 6), accuracy (Equation 7), and f-criterion (Equation 8)[43].

$$\text{Re}\,call = \frac{TP}{TP + FN} \quad (5) \qquad \text{Pr}\,ecision = \frac{TP}{TP + FP} \quad (6)$$

$$ACC = \frac{TN + TP}{TN + FN + FP + TP} \quad (7)$$

$$F\_Measure = \frac{2 \times TN}{T2 \times TP + FP + FN} \quad (8)$$

In these equationships, true positive is shown by TP, true negative is shown by TN, false positive is FP and false negative is FN. A standard dataset for esophageal carcinoma pathology reporting was developed based on International Collaboration on Cancer Reporting (ICCR) approach with the aim of improving cancer patient outcomes and international benchmarking in cancer management. The ICCR convened an international multidisciplinary expert panel to identify the best evidence-based clinical and pathological parameters for inclusion in the gastric cancer [۳۲]. In order to evaluate the proposed method, the relevant features are extracted and then with the help of the desired classification types in the mode without feature selection and with the feature selection, the classification and diagnosis of the disease type is done. At first, each feature will be applied to the category input without selecting the feature. Then, these features are combined in series by applying feature selection. In the following, these evaluations have been made in the criteria presented in the research. To evaluate the absolute value of the size of the features of high frequency details and approximation in low frequency, the discrete wavelet transform has been extracted based on the Daubechies filter bank. The number of extracted features is 300 in the second level wavelet transform. The parameters of recall rate, precision, accuracy, specificity and f-criterion are evaluated in three categories: SVM, KNN and RF. Figure 4 shows the detection results of the detection results for the ICCR database on the wavelet transform features at the first level. Similar to what happened in the morphological features, this time the RF classification has shown the best result in the diagnosis of the disease in the endoscopic image. This superiority in the criteria of recall rate, accuracy, specificity and f-criterion is established as an approximation. This time, in wavelet features as well as morphological features, the evaluation criteria of diagnosis has reached 90% in the best case. It should be noted that the results obtained in the multi-resolution features of wavelet transform were much better than the morphological features. The much larger number of features and also the use of Daubechies filter bank in the disease in the endoscopic image is the cause of this difference in the result. In the feature criterion and F criterion, the measured value in the RF category, which has the best result, has reached 95%. Although the desired result is acceptable, due to the large number of features, there is a possibility of over-training and over-fitting.

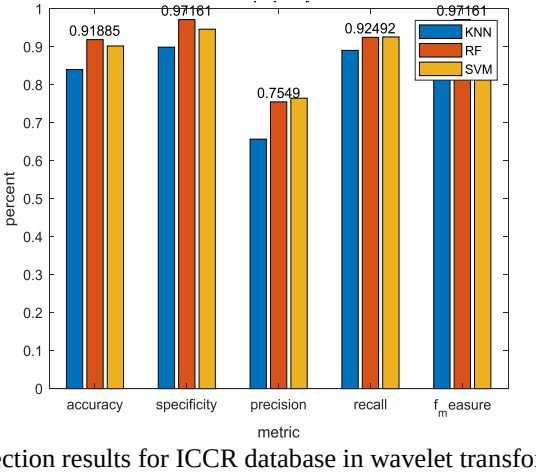

Fig. 4. Detection results for ICCR database in wavelet transform features.

3.1. The Vector of the Series of Features

In this evaluation, the extracted morphological features and wavelet transformation are placed next to each other in series and the corresponding feature vector is made. The length of the feature vector is 325. The parameters of recall rate, precision, accuracy, specificity and f-criterion are evaluated in three categories: SVM, KNN and RF. Figure 5 shows the results of disease diagnosis in the endoscopic image in the ICCR database in the feature series vector. As shown in the results in Figure 5, similar to what happened in the morphological characteristics and discrete wavelet transform, the RF classification has shown the best result in the diagnosis of the disease in the endoscopic image, as in

the previous three cases. This superiority in the criteria of recall rate, accuracy, specificity and f-criterion is established as an approximation.This time, like the morphological characteristics, the diagnostic evaluation criteria has reached 90% in the best case. It should be noted that the results obtained in the multi-resolution features of wavelet transform were much better than the morphological features. The much larger number of features and also the use of Daubechies filter bank in the disease in the endoscopic image is the cause of this difference in the result. In the feature criterion and F criterion, the measured value in the RF category, which has the best result, has reached 99%. Although the desired result is acceptable, due to the large number of features, there is a possibility of over-training and over-fitting. For this purpose and to avoid over fitting in this research, a dimension reduction based on PCA is presented.

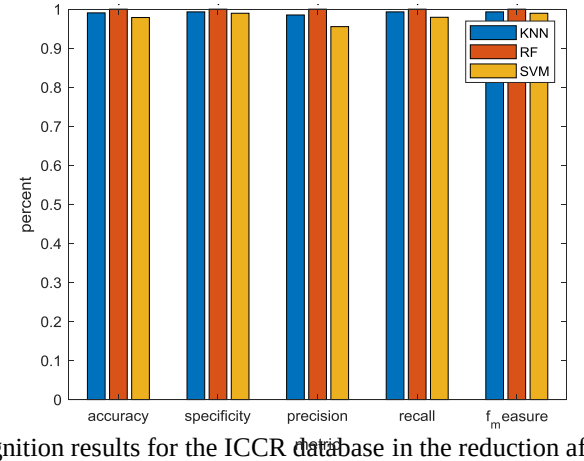

Fig.5. Recognition results for the ICCR database in the reduction after the feature series vector.

3.2. Comparison of Detection Time

By selecting the feature, the speed of diagnosing the disease in the endoscopic image will increase. While the feature vector length is 325 numbers in the series mode, only 65 features are selected in the feature selection mode. Choosing a smaller number of features, in addition to preventing over fitting of the classifications, also improves the evaluation criteria proposed in the research for diagnosis. Also, less number of features can improve the detection speed. In order to evaluate the detection time, the ric-toc command is used. This order is placed before and after the categories. Table 1 shows the comparison of classification and diagnosis time in different categories. The detection time is measured with the system used for simulation. Based on the results obtained in this table, the SVM classifier has a higher speed in diagnosis. Although the RF classifier has shown a better result from the point of view of other evaluation criteria, but because it is in the group classifiers, it has a weaker performance in response and recognition time.

Table 1. Samples of times roman type sizes and styles used for formatting a technical work.

Database	Class type	Before feature (selection seconds)	After selecting the (feature seconds)
ICCR Database	SVM	0.1902	0.1500
	KNN	0.2314	0.1803
	RF	0.2996	0.2408

3.3. Comparison with Other Researchers

The best result obtained in this research belongs to the RF category. Therefore, the results obtained in this research will be compared with other studies that have used a similar database (ICCR database). In these articles, some criteria are reported and others are not reported. The results and criteria reported in these articles will be presented. As can be seen from Table 2, the proposed method shows superior results compared to the presented methods.

\

Table 2. Comparison with other researches.

Reference	Methodology/WL	Performance
[33]	Hybrid Deep Learning Model	Sen:94%
[34]	Texture and Color Enhancement Imaging	Spec:91% Sen: 94.45%
[35]	Deep Learning Model for Disease Prediction Using Gastrointestinal-Endoscopic Images	Spec:93.8% Acc:96/2% Sen: 94.1%

4. CONCLUSION

In this article, the proposed method was evaluated in the diagnosis of gastric cancer in the endoscopic image. Multi-resolution features based on wavelet transform were extracted with Daubechies filter bank. The parameters of recall rate, precision, accuracy, specificity and f-criterion are evaluated in three categories: SVM, KNN and RF. RF classifier has the best result with numerical values higher than 99% in the proposed method in feature selection based on PCA algorithm, the result in disease diagnosis in endoscopic image in ICCR database. The detection speed was also checked in the proposed method in the detection in all three databases. The SVM classifier has classified the disease in the endoscopic image in the shortest time compared to other classifiers in the database.

REFERENCES

6. [1] A. Abbasi, R. Sadeghi, A. Maleki, and G. Balakhani, "**A meta-analysis of factors related to fertility attitudes, desires, and childbearing intentions in Iranian studies,**" *Interdisciplinary Studies in Humanities,* vol. 14, no. 4, pp. 63-92, 2022.
7. [2] M .Emadi, Z. Jafarian Dehkordi, and M. Iranpour Mobarakeh, "**Improving the Accuracy of Brain Tumor Identification in Magnetic Resonanceaging using Super-pixel and Fast Primal Dual Algorithm,**" *International Journal of Engineering*, vol. 36, no. 3, pp. 505-512.۲۰۲۳ ,
8. [3] M. Karimi, M. Harouni, A. Nasr, and N. Tavakoli, "**Automatic lung infection segmentation of covid-19 in CT scan images,**" *Intelligent Computing Applications for COVID-19*, pp. 235-253: CRC Press, 2021.
9. [4] M. Harouni, M. Karimi, A. Nasr, H. Mahmoudi, and Z. Arab Najafabadi, "**Health monitoring methods in heart diseases based on data mining approach: A directional review,**" *Prognostic models in healthcare: Ai and statistical approaches*, pp. 115-159: Springer, 2022.
10. [5] M. Harouni, M. Karimi, and S. Rafieipour, "**Precise segmentation techniques in various medical images,**" *Artificial Intelligence and Internet of Things: Applications in Smart Healthcare*, vol. 117, 2021.
11. [6] F. Mahmudi, M. Soleimani, and M. Naderi, "**Some Properties of the Maximal Graph ofa Commutative Ring,**" *Southeast Asian Bulletin of Mathematics*, vol. 43, no. 4, 2019.
12. [7] A. J. Moshayedi, A. S. Khan, Y. Shuxin, G. Kuan, H. Jiandong, M. Soleimani, and A. Razi, "**E-Nose design and structures from statistical analysis to application in robotic: a compressive review,**" *EAI Endorsed Transactions on AI and Robotics*, vol. 2, no. 1, pp. e1-e1, 2023.
13. [8] A. Rehman, M. Harouni, M. Karimi, T. Saba, S. A. Bahaj, and M. J. Awan, "**Microscopic retinal blood vessels detection and segmentation using support vector machine and Kenearest neighbors,**" *Microscopy research and technique*, vol. 85, no. 5, pp. 1899-1914, 2022.
14. [9] M. Soleimani, M. H. Naderi, and A. R. Ashrafi, "**TENSOR PRODUCT OF THE POWER GRAPHS OF SOME FINITE RINGS,**" *Facta Universitatis, Series :Mathematics and Informatics*, pp. 101-122, 2019.
15. [10] T. Itoh, H. Kawahira, H. Nakashima, and N. Yata, "**Deep learning analyzes Helicobacter pylori infection by upper gastrointestinal endoscopy images,**" *Endoscopy international open*, vol. 6, no. 02, pp. E139-E144, 2018.
16. [11] J. Podlasek, M. Heesch, R. Podlasek, W. Kilisiński, and R. Filip, "**Real-time deep learning-based colorectal polyp localization on clinical video footage achievable with a wide array of hardware configurations,**" *Endoscopy International Open*, vol. 9, no. 05, pp. E741-E748, 2021.
17. [12] M. Karimi, M. Harouni, E. I. Jazi, A. Nasr, and N. Azizi, "**Improving monitoring and controlling parameters for alzheimer's patients based on iomt,**" *Prognostic models in healthcare: Ai and statistical approaches*, pp. 213-237: Springer, 2022.
18. [13] E. Karimi, A. Ebrahimi, and M. R. Tavakoli, "**How optimal PMU placement can mitigate cascading outages blackouts?,**" *International Transactions on Electrical Energy Systems*, vol. 29, no. 6, pp. e12015, 2019.
19. [14] T. Yan ,P. K. Wong, and Y.-Y. Qin, "**Deep learning for diagnosis of precancerous lesions in upper gastrointestinal endoscopy: A review,**" *World Journal of Gastroenterology*, vol. 27, no. 20, pp. 2531, 2021.
20. [15] M. Soleimani, F. Mahmudi, and M. Naderi, "**Some results on the maximal graph of commutative rings,**" *Advanced Studies: Euro-Tbilisi Mathematical Journal*, vol. 16, no. supp1, pp. 21-26, 2023.
21. [16] G. Zhang, M. Wang, and K. Liu, "**Forest fire susceptibility modeling using a convolutional neural network for Yunnan province of China,**" *International Journal of Disaster Risk Science*, vol. 10, no. 3, pp. 386-403, 2019.

22. [17] K. Namikawa, T. Hirasawa, T. Yoshio, J. Fujisaki, T. Ozawa, S. Ishihara, T. Aoki, A. Yamada, K. Koike, and H. Suzuki, "**Utilizing artificial intelligence in endoscopy: a clinician's guide,**" *Expert review of gastroenterology & hepatology*, vol. 14, no. 8, pp. 689-706, 2020.
23. [18] M. Karimi, M. Harouni, and S. Rafieipour, "**Automated medical image analysis in digital mammography,**" *Artificial intelligence and internet of things*, pp. 85-116: CRC Press, 2021.
24. [19] F. Navabifar, and M. Emadi, "**A Fusion Approach Based on HOG and Adaboost Algorithm for Face Detection under Low-Resolution Images,**" *INTERNATIONAL ARAB JOURNAL OF INFORMATION TECHNOLOGY*, vol. 19 ,no. 5, pp. 728-735, 2022.
25. [20] L. A. de Souza Jr, C. Palm, R. Mendel, C. Hook, A. Ebigbo, A. Probst, H. Messmann, S. Weber, and J. P. Papa, "**A survey on Barrett's esophagus analysis using machine learning,**" *Computers in biology and medicine*, vol. 96, pp ,۲۰۳-۲۱۳ . .۲۰۱۸
26. [21] F. Van Der Sommen, S. Zinger, and E. J. Schoon, "**Computer-aided detection of early cancer in the esophagus using HD endoscopy images.**" pp. 216-227.
27. [22] F. Van Der Sommen, S. Zinger, E. J. Schoon, and P. H. De With, "**Supportive automatic annotation of early esophageal cancer using local gabor and color features,**" *Neurocomputing*, vol. 144, pp. 92-106, 2014.
28. [23] A. R. Hassan, and M. A. Haque, "**Computer-aided gastrointestinal hemorrhage detection in wireless capsule endoscopy videos,**" *Computer methods and programs in biomedicine*, vol. 122, no. 3, pp. 341-353, 2015.
29. [24] R. Mendel, A. Ebigbo, A. Probst, H. Messmann, and C. Palm, "**Barrett's esophagus analysis using convolutional neural networks,**" *Bildverarbeitung für die Medizin 2017*, pp :۸۰-۸۵ .Springer, 2017.
30. [25] Z. Zhang, L. Bai, P. Ren, and E. R. Hancock, "**High-order graph matching kernel for early carcinoma EUS image classification,**" *Multimedia Tools and Applications*, vol. 75, no. 7, pp. 3993-4012, 2016.
31. [26] S. Klomp, F. van der Sommen, A.-F. Swager, S. Zinger, E. J. Schoon, W. L. Curvers, and J. J. Bergman, "**Evaluation of image features and classification methods for Barrett's cancer detection using VLE imaging.**" pp. 84-93.
32. [27] L. A. Passos, L. A. de Souza Jr, R. Mendel, A. Ebigbo ,A. Probst, H. Messmann, C. Palm, and J. P. Papa, "**Barrett's esophagus analysis using infinity restricted Boltzmann machines,**" *Journal of Visual Communication and Image Representation*, vol. 59, pp. 475-485, 2019.
33. [28] G. Liu, J. Hua, Z. Wu, T. Meng, M. Sun, P. Huang, X. He, W. Sun, X. Li, and Y. Chen, "**Automatic classification of esophageal lesions in endoscopic images using a convolutional neural network,**" *Annals of translational medicine*, vol. 8, no. 7, 2020.
34. [29] K.-b. Chen, Y. Xuan, A.-j. Lin, and S-.h. Guo, "**Esophageal cancer detection based on classification of gastrointestinal CT images using improved Faster RCNN,**" *Computer Methods and Programs in Biomedicine*, vol. 207, pp. 106172, 2021.
35. [30] V. Seena, and J. Yomas, "**A review on feature extractionand denoising of ECG signal using wavelet transform**." pp. 1-6.
36. [31] J. Gnitecki, and Z. M. Moussavi, "**Separating heart sounds from lung sounds,**" *IEEE Engineering in medicine and biology magazine*, vol. 26, no. 1, pp. 20, 2007.
37. [32] A. K. Lam, M. J. Bourke ,R. Chen, R. Fiocca, F. Fujishima, S. Fujii, M. Jansen, P. Kumarasinghe, R. Langer, and S. Law, "**Dataset for the reporting of carcinoma of the esophagus in resection specimens: recommendations from the International Collaboration on Cancer Reporting,**" *Human Pathology*, vol. 114, pp. 54-65, 2021.
38. [33] M. S. Ayyaz, M. I. U. Lali, M. Hussain, H. T. Rauf, B. Alouffi, H. Alyami, and S. Wasti, "**Hybrid deep learning model for endoscopic lesion detection and classification using endoscopy videos,**" *Diagnostics*, vol. 12, no. 1, pp. 43, 2021.
39. [34] M. Sugimoto, Y. Kawai, Y. Akimoto, M. Hamada, E. Iwata, M. Murata, H. Mizuno, R. Niikura, N. Nagata, and M. Fukuzawa, "**Third-Generation High-Vision Ultrathin Endoscopy Using Texture and Color Enhancement Imaging and Narrow-Band Imaging to Evaluate Barrett's Esophagus,**" *Diagnostics*, vol. 12, no. 12, pp. 3149, 2022.
40. [35] S. Iyer, D. Narmadha, G. N. Sundar, S. J. Priya, and K. M. Sagayam, "**Deep Learning Model for Disease Prediction Using Gastrointestinal-Endoscopic Images.**" pp. 133-137.
41. [36] F. Mahmudi, M. Soleimani, and M. Naderi, "**Some Properties of the Maximal Graph of a Commutative Ring**," *Southeast Asian Bulletin of Mathematics*, vol. 43, no. 4, 2019.
42. [37] A. J. Moshayedi *et al.*, "**E-Nose design and structures from statistical analysis to application in robotic: a compressive review**," *EAI Endorsed Transactions on AI and Robotics*, vol. 2, no. 1, pp. e1-e1, 2023.
43. [38] B. Heidari and M. Ramezanpour, "**Reduction of intra-coding time for HEVC based on temporary direction map**," *Journal of Real-Time Image Processing*, vol. 17, pp. 567-579, 2020.
44. [39] E. Karimi and A. Ebrahimi, "**Probabilistic transmission expansion planning considering risk of cascading transmission line failures,**" *International Transactions on Electrical Energy Systems*, vol. 25, no. 10, pp. 2547-2561, 2015.
45. [40] E. Karimi and A. Ebrahimi, "**Considering risk of cascading line outages in transmission expansion planning by benefit/cost analysis**," *International Journal of Electrical Power & Energy Systems*, vol. 78, pp. 480-488, 2016.
46. [41] N. Najafabadi and M. Ramezanpour, "**Mass center direction-based decision method for intraprediction in HEVC standard,**" *Journal of Real-Time Image Processing*, vol. 17, no. 5, pp. 1153-1168, 2020.
47. [42] A. Rehman, M. Harouni, F. Zogh, T. Saba, M. Karimi, and G. Jeon, "**Detection of Lung Tumors in CT Scan Images using Convolutional Neural Networks,**" *IEEE/ACM Transactions on Computational Biology and Bioinformatics*, 2023.
48. [43] Y. Saberi, M. Ramezanpour, and R. Khorsand, "**An efficient data hiding method using the intra prediction modes in HEVC,**" *Multimedia Tools and Applications*, vol. 79, pp. 33279-33302, 2020.

49. [44] R. G. Anaraky *et al.*, "**Older and younger adults are influenced differently by dark pattern designs,**" *arXiv preprint arXiv:2310.03830*, 2023.
50. [45] M. Emadi, M. Karimi, and F. Davoudi, "**A Review on Examination Methods of Types of Working Memory and Cerebral Cortex in EEG Signals,**" *Majlesi Journal of Telecommunication Devices*, vol. 12, no. 3, 2023.